

**UAV-BASED RGB/NIR AERIAL IMAGING FOR THE  
DETECTION OF *Ganoderma* DISEASE IN  
OIL PALM PLANTATION**

**EZZATI BAHROM**

**INSTITUTE OF GRADUATE STUDIES  
UNIVERSITY OF MALAYA  
KUALA LUMPUR**

**2018**

**UAV-BASED RGB/NIR AERIAL IMAGING FOR THE  
DETECTION OF *Ganoderma* DISEASE IN  
OIL PALM PLANTATION**

**EZZATI BAHROM**

**DISSERTATION SUBMITTED IN FULFILMENT OF THE  
REQUIREMENTS FOR THE DEGREE OF  
MASTER OF PHILOSOPHY**

**INSTITUTE OF GRADUATE STUDIES  
UNIVERSITY OF MALAYA  
KUALA LUMPUR**

**2018**

**UNIVERSITY OF MALAYA**  
**ORIGINAL LITERARY WORK DECLARATION**

Name of Candidate: Ezzati Bahrom

Matric No: HGT150003

Name of Degree: Master of Philosophy

Title of Dissertation: UAV-Based RGB/NIR Aerial Imaging for the Detection of  
*Ganoderma* Disease in Oil Palm Plantation

Field of Study: Earth Science (*Air-Ocean-Land Interactions*)

I do solemnly and sincerely declare that:

- (1) I am the sole author/writer of this Work;
- (2) This Work is original;
- (3) Any use of any work in which copyright exists was done by way of fair dealing and for permitted purposes and any excerpt or extract from, or reference to or reproduction of any copyright work has been disclosed expressly and sufficiently and the title of the Work and its authorship have been acknowledged in this Work;
- (4) I do not have any actual knowledge nor do I ought reasonably to know that the making of this work constitutes an infringement of any copyright work;
- (5) I hereby assign all and every rights in the copyright to this Work to the University of Malaya ("UM"), who henceforth shall be owner of the copyright in this Work and that any reproduction or use in any form or by any means whatsoever is prohibited without the written consent of UM having been first had and obtained;
- (6) I am fully aware that if in the course of making this Work I have infringed any copyright whether intentionally or otherwise, I may be subject to legal action or any other action as may be determined by UM.

Candidate's Signature

Date:

Subscribed and solemnly declared before,

Witness's Signature

Date:

Name:

Designation:

# UAV-BASED RGB/NIR AERIAL IMAGING FOR THE DETECTION OF *Ganoderma* DISEASE IN OIL PALM PLANTATION

## ABSTRACT

*Ganoderma* disease in oil palm caused by *Ganoderma* spp. fungi have caused significant losses of Malaysia's economic income. Advances in remote sensed imagery and image processing using unmanned aerial vehicle (UAV) for *Ganoderma* disease detection could be developed to reduce operating cost and time as well as cover wider oil palm areas. This study examines the performance of red-green-blue (RGB) and near-infrared (NIR) digital orthophoto image acquired using modified digital cameras mounted on the UAV for aerial detection of *Ganoderma* disease in oil palm. The orthophoto images were filtered using eight adaptive filters with window sizes of  $7 \times 7$ ,  $9 \times 9$  and  $11 \times 11$ . The filtered orthophoto images then were processed using three supervised image classifiers: Maximum Likelihood (ML), Mahalanobis Distance (MD) and Neural Net (NN). The classifiers were used to classify the *Ganoderma* disease severities into Experiment 1: T0 (healthy), T1 (mild), T2 (moderate) and T3 (severe); and Experiment 2: healthy and unhealthy. The classification outputs were assessed using a confusion matrix. Best result was obtained from Bit Error filter with  $9 \times 9$  window size using the NN algorithm with an overall accuracy of 62.41% and a Kappa coefficient of 0.3890. This study demonstrated classification from UAV-based imagery can be improved using filters for *Ganoderma* disease detection mapping in oil palm plantation.

**Keywords:** *Ganoderma* disease, digital aerial orthophoto, supervised classification

## IMEJ RGB/NIR BERASAKAN UAV UNTUK PENGESANAN PENYAKIT *Ganoderma* DALAM PERLADANGAN KELAPA SAWIT

### ABSTRAK

Penyakit *Ganoderma* kelapa sawit yang disebabkan oleh kulat *Ganoderma spp.* telah mengakibatkan kerugian besar terhadap ekonomi Malaysia. Kemajuan dalam pengimejan dan pemrosesan imej yang dikesan menggunakan kenderaan udara tanpa pemandu (UAV) untuk pengesanan penyakit *Ganoderma* dapat dibangunkan untuk mengurangkan kos dan masa operasi serta meliputi kawasan kelapa sawit yang luas. Kajian ini mengkaji prestasi imej digital ortofoto merah-hijau-biru (RGB) dan inframerah dekat (NIR) yang diperoleh menggunakan kamera digital yang telah diubahsuai pada UAV untuk mengesan penyakit *Ganoderma* dari udara pada kelapa sawit. Imej ortofoto telah dituras menggunakan lapan penyesuaian turas dengan saiz tettingkap  $7 \times 7$ ,  $9 \times 9$  dan  $11 \times 11$ . Imej ortofoto yang telah dituras kemudian diproses menggunakan tiga klasifikasi imej yang diselia: Maximum Likelihood (ML), Mahalanobis Distance (MD) dan Neural Net (NN). Pengelasan digunakan untuk mengelaskan tahap keterukan penyakit *Ganoderma* pada Eksperimen 1: T0 (sihat), T1 (ringan), T2 (sederhana) dan T3 (teruk); dan Eksperimen 2: sihat dan tidak sihat. Pengelasan klasifikasi dinilai menggunakan matriks kekeliruan. Hasil terbaik diperoleh daripada pengelas Bit Error dengan saiz tettingkap  $9 \times 9$  menggunakan algoritma NN dengan ketepatan keseluruhan 62.41% dan pekali Kappa 0.3890. Kajian ini menunjukkan bahawa klasifikasi daripada imej berasaskan UAV dapat ditingkatkan menggunakan penapis untuk pemetaan penyakit *Ganoderma* dalam ladang kelapa sawit.

**Kata kunci:** Penyakit *Ganoderma*, digital ortofoto udara, klasifikasi diselia

## ACKNOWLEDGEMENTS

In the name of Allah, the Most Gracious and Most Merciful. Alhamdulillah and I pray gratitude to Him for giving me the wisdom and determination to complete this dissertation.

I would like to express my deepest gratitude to my main supervisor, Dr. Nisfariza Mohd Noor for her motivation and support that made it possible for me to work on a topic that was of great interest to me. Her excellent guidance throughout my MPhil journey is much appreciated.

I would also like to acknowledge with much appreciation to Associate Professor Dr. Siti Aisah Alias and Dr. Idris Abu Seman for their immense interest in my topic of research, for their kind words and suggestions.

I am gratefully indebted to Mr. Mohamad Izzuddin Anuar for finding out time for being ever so kind to help and giving inputs and kind advice regarding the topic of my research. Special thanks also go to the technical staff of *Ganoderma* and Diseases Research for Oil Palm (GANOROP) Unit, Malaysian Palm Oil Board (MPOB) for their assistance that helped me along the way.

I thank my fellow colleagues in UMSerge and GIS Unit, SWM for their support and encouragement throughout my dissertation preparation and helping me keep things in perspective.

My sincere thanks also go to my family, especially both of my parents and parents-in-law for their constant prayers and support. Finally, I would like to thank my husband, Afiq and our child I'm carrying for their understanding and been continually supportive, together experienced all the ups and downs of my research journey.

## TABLE OF CONTENTS

Abstract .....	iii
Abstrak .....	iv
Acknowledgements .....	v
Table of Contents .....	vi
List of Figures .....	x
List of Tables .....	xii
List of Symbols and Abbreviations .....	xiii
List of Appendices .....	xv
<b>CHAPTER 1: INTRODUCTION .....</b>	<b>1</b>
1.1 Overview .....	1
1.2 Problem Statement .....	2
1.3 Research Aim .....	3
1.4 Research Objectives .....	4
1.5 Research Questions .....	4
1.6 Significance of Study .....	5
1.7 Structure of Thesis.....	6
<b>CHAPTER 2: LITERATURE REVIEW .....</b>	<b>7</b>
2.1 The Oil Palm .....	7
2.2 Oil Palm Cultivation .....	7
2.3 Oil Palm Morphology and Botany .....	8
2.3.1 The Root System .....	9
2.3.2 The Stem .....	10

2.3.3 The Leaf .....	10
2.3.4 The Fruit .....	11
2.4 Palm Oil and Palm Kernel Oil Products .....	12
2.5 Pests and Diseases of Oil Palm .....	12
2.5.1 Oil Palm Pests .....	12
2.5.2 Oil Palm Diseases .....	13
2.6 <i>Ganoderma</i> Disease of Oil Palm .....	13
2.7 <i>Ganoderma</i> Symptoms and Disease Development .....	15
2.8 Control and Treatment of <i>Ganoderma</i> Disease .....	16
2.9 Remote Sensing Principles .....	18
2.10 The Electromagnetic Spectrum .....	18
2.11 Remote Sensing Sensors .....	19
2.12 Multispectral Remote Sensing .....	20
2.12.1 Spatial, Spectral and Temporal Characteristics .....	21
2.13 Multispectral Image Analysis .....	21
2.14 Remote Sensing Platforms .....	22
2.15 Unmanned Aerial Vehicle (UAV) .....	23
2.16 Plant Signal Interaction .....	24
2.17 Vegetation Properties .....	25
2.18 Remote Sensing for Precision Agriculture .....	26
2.20 Application of Remotely Sensed Sensors in <i>Ganoderma</i> Disease Identification .....	27
2.20.1 Hyperspectral Remote Sensing in <i>Ganoderma</i> Disease Detection .....	27
2.20.2 Multispectral Remote Sensing in <i>Ganoderma</i> Disease Detection .....	28
2.21 UAV-Based Platform in Oil Palm Monitoring .....	29



<b>CHAPTER 3: METHODOLOGY .....</b>	<b>33</b>
3.1 Study Area .....	33
3.2 Ground Data Collection .....	34
3.3 Classification of Treatments .....	36
3.4 Flight Mission .....	39
3.4.1 Platform .....	39
3.4.2 Sensor .....	40
3.4.3 GPS Equipment .....	41
3.5 Flight Planning .....	42
3.6 Image Pre-Processing .....	43
3.7 Identification of Regions of Interest .....	44
3.8 GIS as Input for Remote Sensing Interpretation .....	49
3.9 Image Processing .....	50
3.9.1 Filtering .....	50
3.10 Supervised Classification .....	51
3.10.1 Maximum Likelihood (ML) .....	51
3.10.2 Mahalanobis Distance (MD) .....	52
3.10.3 Neural Net (NN) .....	53
3.11 Accuracy Assessment .....	55
3.12 Confusion Matrix .....	55
3.12.1 Overall Accuracy and Kappa Coefficient .....	55
3.12.2 Producer Accuracy and User Accuracy .....	57
<b>CHAPTER 4: RESULTS .....</b>	<b>60</b>
4.1 Adaptive Filters .....	60
4.1.1 Lee Filter .....	63
4.1.2 Enhanced Lee Filter .....	65

4.1.3 Frost Filter .....	64
4.1.4 Enhanced Frost Filter .....	64
4.1.5 Gamma Filter .....	65
4.1.6 Kuan Filter .....	65
4.1.7 Local Sigma Filter .....	66
4.1.8 Bit Error Filter .....	66
4.2 Summary .....	71
<b>CHAPTER 5: DISCUSSION .....</b>	<b>73</b>
5.1 Introduction .....	73
5.2 Multispectral Bands versus Hyperspectral Bands .....	75
5.3 Training Samples Classification .....	76
5.4 Window Size of the Adaptive Filter .....	77
5.5 Supervised Classification .....	78
5.6 Classification Results .....	79
5.7 Conclusion .....	80
<b>CHAPTER 6: CONCLUSION .....</b>	<b>81</b>
6.1 Introduction .....	81
6.2 Recommendations .....	83
6.3 Future Work .....	84
6.4 Conclusion .....	85
References .....	86
List of Publication and Paper Presented .....	101
Appendix .....	102

## LIST OF FIGURES

Figure 2.1: The different types of roots of an adult oil palm root system .....	10
Figure 2.2: Cross-longitudinal section of oil palm fruit varieties (a) Dura, (b) Tenera and (c) Pisifera, showing the relative proportions of shell, kernel and pulp .....	12
Figure 2.3: Basidiocarps at the basal stem of oil palm .....	14
Figure 2.4: The rotten oil palm stem base affected by <i>Ganoderma</i> disease .....	15
Figure 2.5: Technologies developed by MPOB for <i>Ganoderma</i> disease detection ...	18
Figure 2.6: Electromagnetic spectrum, with shortwave energy depicted to the left and long wave to the right .....	19
Figure 2.7: Reflectance of water, soil and vegetation in different wavelengths .....	22
Figure 2.8: The interaction of leaf structure with visible and infrared radiation. Red and blue absorbed largely for photosynthesis .....	25
Figure 3.1: The study site location in yellow polygon .....	34
Figure 3.2: The overall flow chart of the methodology .....	35
Figure 3.3: Four classes of DSI that infected the oil palms .....	37
Figure 3.4: Swinglet with modified compact camera .....	39
Figure 3.5: Canon IXUS 220HS camera that's mounted on Swinglet .....	40
Figure 3.6: The Garmin GPS equipment .....	42
Figure 3.7: Flight lines for Swinglet UAV .....	43
Figure 3.8: UAV-based multispectral image of oil palm plantation. The yellow box indicates the study area. (a) Digital orthophoto mosaic image of RGB; (b) Digital orthophoto mosaic image of NIR .....	44
Figure 3.9: Examples of oil palm crown for each oil palm DSI .....	46
Figure 3.10: ROI tool that shows the list for training and test samples.....	48
Figure 3.11: Manual classification of different polygon areas for each class based on the oil palm location .....	48
Figure 3.12: Overlaying of 120 points of ground truth in GIS for NIR image .....	49
Figure 3.13: The selected classes for ML parameters .....	54

Figure 3.14: (a) RGB colour image of the oil palm captured by the UAV; (b) Classification thematic map produced by the ML algorithm .....	54
Figure 3.15: Classes parameters sets for training and test samples .....	58
Figure 3.16: Class confusion matrix produces using confusion matrix .....	59
Figure 4.1: RGB and NIR original images without using filter in Experiment 1	61
Figure 4.2: RGB and NIR original images without using filter in Experiment 2	62
Figure 4.3: Results of RGB image with selected window sizes, filters and classifier in Experiment 1 .....	67
Figure 4.4: Results of RGB image with selected window sizes, filters and classifier in Experiment 1 .....	68
Figure 4.5: Results of RGB image with selected window sizes, filters and classifier in Experiment 1 .....	69
Figure 4.6: Results of RGB image with selected window sizes, filters and classifier in Experiment 1 .....	70

## LIST OF TABLES

Table 2.1: Total area of oil palm cultivation in Peninsular Malaysia .....	8
Table 2.2: Comparison of UAV with other manned airborne and satellite platforms .....	23
Table 2.3: Summary of remotely sensed sensors and methods used in oil palm studies .....	32
Table 3.1: <i>Ganoderma</i> Disease Severity Index (DSI) and visual symptoms for Experiment 1 .....	38
Table 3.2: <i>Ganoderma</i> Disease Severity Index (DSI) and visual symptoms for Experiment 2 .....	38
Table 3.3: Specification of UAV Swinglet .....	39
Table 3.4: Canon IXUS 220HS technical specifications .....	40
Table 3.5: Numbers of training samples (ROI) and test samples, which were manually generated in pixels for Experiment 1 .....	47
Table 3.6: Numbers of training samples (ROI) and test samples, which were manually generated in pixels for Experiment 2 .....	54
Table 3.7: The interpretation of Kappa coefficient .....	56
Table 4.1: The overall accuracy and Kappa coefficient obtained from Experiment 1 and Experiment 2 .....	72

## LIST OF SYMBOLS AND ABBREVIATIONS

AISA	:	Airborne Imaging Spectrometer for Applications
BSR	:	Basal Stem Rot
D×P	:	<i>dura × pisifera</i>
DSI	:	Disease Severity Index
DTM	:	Digital Terrain Model
EM	:	Electromagnetic
ENVI	:	Environment for Visualizing Images
FAO	:	Food and Agriculture Organization
GCP	:	Ground Control Point
GDP	:	Gross Domestic Product
GIS	:	Geographical Information System
GPS	:	Global Position System
GSD	:	Ground Sampling Distance
GSM	:	<i>Ganoderma</i> Selective Medium
IMU	:	Inertial Measurement Unit
LARS	:	Low Altitude Remote Sensing
LiDAR	:	Light Detection and Ranging
MD	:	Mahalanobis Distance
Mha	:	Million hectares
ML	:	Maximum Likelihood
MPOB	:	Malaysian Palm Oil Board
MPOPC	:	Malaysian Palm Oil Promotion Council
NIR	:	Near Infrared
NN	:	Neural Net

R&D	:	Research and Development
RADAR	:	Radio Detection and Ranging
RGB	:	Red-Green-Blue
ROI	:	Region of Interest
SWIR	:	Short Wave Infrared
TIR	:	Thermal Infrared
UAV	:	Unmanned Aerial Vehicle
UTM	:	Universal Transverse Mercator

University of Malaya

**LIST OF APPENDICES**

Appendix A ..... 102

Appendix B ..... 104

University of Malaya



## CHAPTER 1: INTRODUCTION

### 1.1 Overview

The oil palm tree (*Elaeis guineensis* Jacq.) is an important tree, which has been one of the world's major sources of edible oil. The oil palm occupies 16 million hectares (Mha) globally and oil palm industry contributes to the gross domestic product (GDP) for agricultural sector growth. Malaysia and Indonesia cultivate oil palm in larger scale due to its high yield and low production cost of palm oil (Kian *et al.*, 2013).

The most common manifestation of the disease that attacks oil palm is the *Ganoderma* disease. This disease decays the root system progressively and the lower stem induces disease symptoms (Rees *et al.*, 2009). A white rot fungus *Ganoderma* causes this disease. In Malaysia, *Ganoderma boninense* is the major pathogen since *Ganoderma* is a regional disease. This soil-borne fungus attack from the palm roots and slowly spread to the stem and bole system of the palm trunk (Idris, 2004).

*Ganoderma* disease that attacks oil palm caused an effect on the palm oil production in Malaysia. The disease can threaten the industry by shortening the lifespan of oil palm trees and affecting the yield and quality of the fruit. *Ganoderma* disease early detection is necessary for disease management as currently there is a barely effective treatment to control this disease (Liaghat *et al.*, 2014).

Image capturing using satellite and airborne is growing in number as it is commonly used for precision agriculture or site-specific crop management that includes crops monitoring and fertilizer management with the aid of remote sensors. Each system delivers unique capabilities that are suitable for specific uses to increase crop yields (Zarco-Tejada *et al.*, 2016).

The unmanned aerial vehicle (UAV) platform with a better combination of spatial and temporal resolution has turned out to be industrially accessible for diverse applications. The advantages of UAV are their lower cost and represent a minor threat or damage in case of malfunction compared to piloted airborne and satellite platforms (Saberioon *et al.*, 2014). The uses of the UAV can overcome the difficulties related to spatial and temporal resolution since the images taken from UAV platform are likely to collect detailed geospatial information in real-time (Fornace *et al.*, 2014).

Plant diseases can affect the quality and quantity of the crop production. The naked eye method used to identify the disease requires the expert to detect the changes in leaf colour that involves continuous monitoring; time-consuming and not practical in large fields (Ghaiwat & Arora, 2014).

Detection and control of *Ganoderma boninense* strategies have widespread due to the advanced technologies. Thus, the purpose of this study is to demonstrate the UAV capability of collecting image data efficiently to determine the separability between classes of healthy and diseased palms in the oil palm plantation.

## 1.2 Problem Statement

*Ganoderma* disease is the most common disease that attacks and caused major losses in the South East Asia oil palm industry. The causal pathogen is caused by *Ganoderma spp.* that attack the palm stem rot. It has been identified that *Ganoderma boninense* is the major pathogen on oil palm in Malaysia (Idris, 2004).

In 2011, 3.71% or 60,000 hectares of oil palm plantation in Peninsular Malaysia were lost due to *Ganoderma* disease incidence with estimated losses of RM 1.8 billion. The total area expected to be affected by *Ganoderma* will rise to about 443,430 hectares or 65.6 million palm trees with approximately RM 11.25 billion losses by the year 2020

(Roslan & Idris, 2012). Moreover, this fatal disease can cause losses up to 80% after repeated planting cycles (Flood *et al.*, 2000).

Monitoring for *Ganoderma* disease in oil palm plantation is time and labour consuming. Large areas of oil palm plantations require an airborne monitoring system to locate *Ganoderma* disease hot spots for fast and effective control measures. It is crucial to develop an early detection tool in order to achieve a successful disease management and save cost based on airborne technology. From the newly emerging method of remote sensing using a UAV system, early detection and assessment of the disease symptoms are vital to control and manage the oil palm crop. This is due to there is more than 50% of the oil palm plantation in Peninsular Malaysia that being attacked with *Ganoderma* disease that requires near real-time detection. The in-depth study is required to identify a suitable method that utilized fixed-wing UAV multispectral image for aerial detection of *Ganoderma* disease in oil palm.

### **1.3 Research Aim**

The aim of this study is to assess the performance of image-based red-green-blue (RGB) and near-infrared (NIR) from fixed-wing UAV captured over selected oil palm plantation with varying levels of *Ganoderma* disease severity indexes, and to determine the best classification technique for the detection of the disease.

#### 1.4 Research Objectives

In this study, the performance of fixed-wing Swinglet UAV using Canon IXUS 220HS image products was assessed in response to the *Ganoderma* disease varying levels in oil palm plantation. Three objectives were established to achieve the study aim:

1. to examine the performance of classification techniques for the detection of *Ganoderma* disease in oil palm;
2. to compare between RGB and NIR image performance using three different supervised classifiers;
3. to assess the effects of different adaptive filters on the classification performance for the detection of *Ganoderma* disease in oil palm.

#### 1.5 Research Questions

To achieve the objectives, the following research questions are defined:

1. Which supervised classification technique (Maximum Likelihood (ML), Mahalanobis Distance (MD) or Neural Net (NN)) gives the best result in the detection of *Ganoderma* disease in oil palm?
2. Which image (RGB or NIR) is outperforming in detecting the *Ganoderma* disease using three different supervised classifiers?
3. Which adaptive filters show the best result on the classification performance for the detection of *Ganoderma* disease in oil palm?

## 1.6 Significance of Study

This study is significant mainly to the oil palm industry and potentially important for the agricultural industries in Malaysia. It is important for the oil palm management to assess for the spread of *Ganoderma* disease in the oil palm plantation areas. The application of UAV images in precision agriculture is vital to control the spread of *Ganoderma* disease in mature palms while sustaining the agriculture production.

In this study, the RGB and NIR images were classified separately using ML, MD and NN classifiers. The classification results are represented in thematic images in two sets of experiments, which in Experiment 1, the T0 is represented by the green colour, T1 by the purple colour, T2 by the yellow colour and T3 by the red colour. Meanwhile, for Experiment 2, the healthy class represented in green colour and the unhealthy class represented in red colour.

The success of the detection of *Ganoderma* disease infection helps reduce the loss of oil palm crops through the mapping of *Ganoderma* disease from UAV images and perhaps eradication of the disease. This is important as the Malaysian oil palm plantation sector is recognised as having a high demand for nutrients. From this study, the accuracy assessment of supervised classification techniques will be discovered from the UAV platform towards the detection of *Ganoderma* disease through the oil palm crown. The novelty of this study is to provide an understanding of the analysis of UAV-based image product in *Ganoderma* disease that affecting the oil palm area by comparing different supervised classifiers by their performances will make a significant contribution to future precision agriculture research. A competent classifier is needed to extract and produce quality information from remote sensing images.

## 1.7 Structure of Thesis

The material in this thesis is organized in six chapters, divided into three broad topic areas: (1) *Ganoderma* disease in oil palm plantation, (2) UAV as a remote sensing platform and (3) the application of supervised classification techniques. Brief explanations in each chapter are listed in this section.

Chapter 1 contains an introduction to the study and the problem statement. Research identification will be divided into research objectives, research questions and the significance of the study.

Chapter 2 presents broad literature reviews that are useful in this study. A brief overview of the oil palm and the background symptoms of *Ganoderma* disease also presented. Remote sensing principles and recent studies on UAV products in agricultural used will also be discussed further in this chapter.

Chapter 3 consists of a detailed description of the methods used in this study. In general, this study is arranged into three segments: data acquisition, data processing, and data analysis. A thorough flowchart, process for each segment and approaches used to complete the objectives are specifically described in this chapter.

Chapter 4 comprises detailed results of each step in this study. From the data obtained from fieldwork, data processing and up to analysis of the results upon achieving the output of the UAV-based image product.

Chapter 5 consists of general and technical discussion regarding the results based on the findings of this study.

Finally, Chapter 6 encompasses the conclusions of the research chapters and the summary of the results. Recommendations also contained in this chapter.

## CHAPTER 2: LITERATURE REVIEW

### 2.1 The Oil Palm

Oil palm, *Elaeis guineensis* Jacq., is an unbranched monoecious plant that belongs to the genus *Elaeis* that was originated from Africa, particularly in West Africa (Verheye, 2010). Oil palm is primarily produced in Malaysia and Indonesia is one of the important sources of vegetable oil in the world that provide nearly 90% of the oil entering the international trade (Corley & Tinker, 2015; Rivera-Méndez *et al.*, 2017). Oil palm vegetative oil is grown for its industrial production has the highest productivity compared to other oleaginous crops (Verheye, 2010; Barcelos *et al.*, 2015). China, European Union, Pakistan, India, Japan and Bangladesh are the primary markets for palm oil international trade (Vollmann & Rajcan, 2009).

Oil palm was first introduced in Malaysia in 1875 as an ornamental plant and become commercial planting in 1917. The Malaysian government has encouraged the expansion of oil palm in the 1960s due to its rapid expansion and introduced the clearing of land for oil palm plantations. Currently, Malaysia is the second largest grower of palm oil with a yearly production of 19.96 million tonnes in 2015, meanwhile Indonesia with palm oil production of 33.6 million tonnes (MPOB, 2016a).

### 2.2 Oil Palm Cultivation

Oil palm requires deep or peat soil and needs high temperature and continuous moisture throughout the year since it is a tropical tree crop (Verheye, 2010). Malaysia only had 400 ha plantation in 1921. The area increased to 0.6 million hectares in 1975 to 5.4 million hectares in 2014 (MPOB, 2015). Table 2.1 shows the oil palm cultivation area, that being occupied in Peninsular Malaysia as at December 2015.

**Table 2.1: Total area of oil palm cultivation in Peninsular Malaysia**

<i>State</i>	<i>Area (ha)</i>
Johor	738,583
Pahang	725,739
Perak	398,318
Negeri Sembilan	177,741
Terengganu	172,587
Kelantan	151,973
Selangor	137,336
Kedah	87,244
Melaka	54,603
Penang	14,447
Perlis	295

**Source: MPOB, 2016b**

Malaysian Palm Oil Board (MPOB) and Malaysian Palm Oil Promotion Council (MPOPC) being the main institutions that aimed to increase quality and productivity and expanding export markets of the oil palm industry. MPOB's role is to make sure the development in the palm oil industry by involving palm oil quality control and its products through research and development (R&D). Meanwhile, MPOPC performs on the palm oil market promotion, especially in the export markets (Shome & Sharma, 2015).

### **2.3 Oil Palm Morphology and Botany**

The oil palm tree is a member of the family *Palmae*, subfamily *Cocoideae*, and genus *Elaeis*. The genus contains three main species: *E. guineensis* (commercial red oil palm) from Africa, *E. oleifera* (American oil palm) and *E. odora* (grown in the Amazon) both from South America (Verheye, 2010). Of the three species, the *E. guineensis* is the worldwide grown crop and cultivated on a wide scale compare to *E. oleifera* that have lower oil content (Idris, 1999).



Oil palm pollination is primarily by insects. The pollinating weevil *Elaeidobius kamerunicus*, imported from Cameroon, Africa was first introduced in Malaysia by the middle of 1981 to improve pollination and to increase fruit set (Lajis *et al.*, 1985; Rizuan *et al.*, 2013). Before this time, oil palms in the region require artificial pollination or wind pollinated. Weevil feeds on the palm male inflorescence tissues and male flowers to complete the entire life cycle. The weevil's pollination efficiency depends on its ability to transfer pollens while visiting both male and female oil palm flowers during anthesis (Lajis *et al.*, 1985).

The oil palm growing in South East Asia requires low rainfall and high altitude for growth development. Oil palm is a rain-fed plantation crop that requires an average of 1780-2280 mm annual rainfall that is evenly distributed throughout the year with optimal temperatures between 24 and 30 °C (Mukherjee & Sovacool, 2014). The annual rainfall plays a major role in its growth and yield, apart from soil fertility and management inputs (Haniff *et al.*, 2014). The oil palm tree's height can reach 15-18 m and up to 30 m in a dense forest (Barcelos, 2015). The four main parts of the palm tree include root, stem, leaves or fronds and fruit (Roslan *et al.*, 2004).

### **2.3.1 The Root System**

Oil palm is a perennial monocot and has an extensive root system that is a greater part of nutrients uptake. The root structure starts with primary roots that go down profoundly from the trunk base. The primary roots will continue to produce secondary, tertiary and quaternary roots around the tree (Verheye, 2010). The root system supports the palm tree to stand upright on the ground for minerals and water uptake from the soil (Hartley, 1988). Figure 2.1 shows the different appearance types of roots.

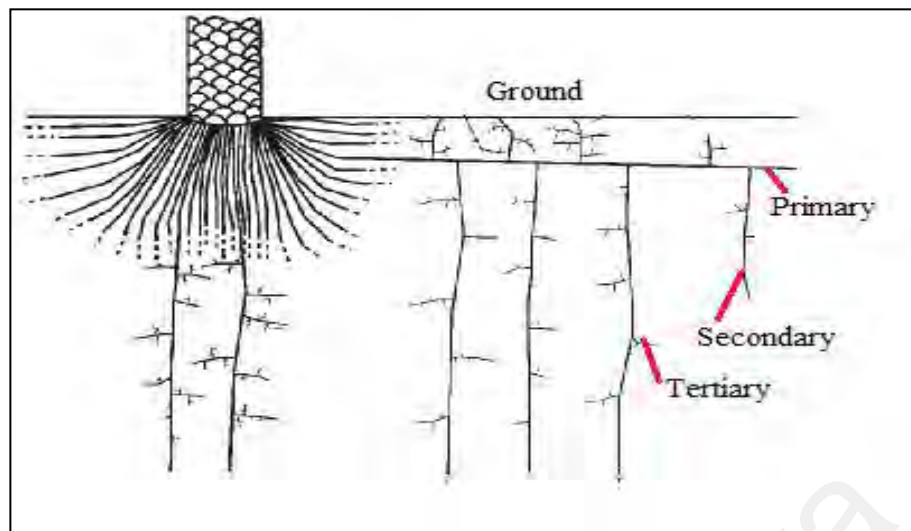


**Figure 2.1: The different types of roots of an adult oil palm root system**  
**Source: Corley & Tinker, 2008**

### 2.3.2 The Stem

The oil palm has no branches, but it has a trunk or stripe that is the stem of the palm (FAO, 2002). The oil palm stem consists of the cortex that is formed by the extension of the leaf bases. The stem function is being a support, vascular and storage organ. The vascular bundles within the stem supply water and nutrients to the fronds and photosynthetic absorb to the roots (Corley & Tinker, 2015).

### 2.3.3 The Leaf

The meristem or apical bud produces 40-60 leaves which comprise the petiole, rachis, and leaflets; each remains encircle for 2 years and opens into a middle 'spear'. At 2-4 years of age, the number of leaves produced annually increases to between 30 and 40. The developing leaf base completely encloses the stem apex. A mature palm leaf is pinnate and have overgrown linear leaflets on each side of the leaf stalk. There are 250 - 300 leaflets per fully developed leaf and the sizes are up to 1.3 m long and 6 cm broad (Corley & Tinker, 2015).

### 2.3.4 The Fruit

The oil palm fruit yield is of greatest economic significance. The preferred species grown in South East Asia, *E. guineensis* has three fruit forms, *dura*, *tenera*, and *pisifera*. The extractable oil from *E. guineensis* produces more productive oil compared to coconut, peanut, soya bean and sunflower (Idris, 1999).

The character of these three fruits can be distinguished based on its shell thickness: (i) *Dura*, thick-shelled, (ii) *Pisifera*, shellers, and (iii) *Tenera*, a thin-shelled. The *tenera* is a hybrid between *dura* × *pisifera* parents, planted commercially due to its thick mesocarp and thin shell, and produces 30% more oil than the *dura* (MPOB, 2015). Figure 2.2 shows the cross-longitudinal section of the three oil palm fruit varieties.

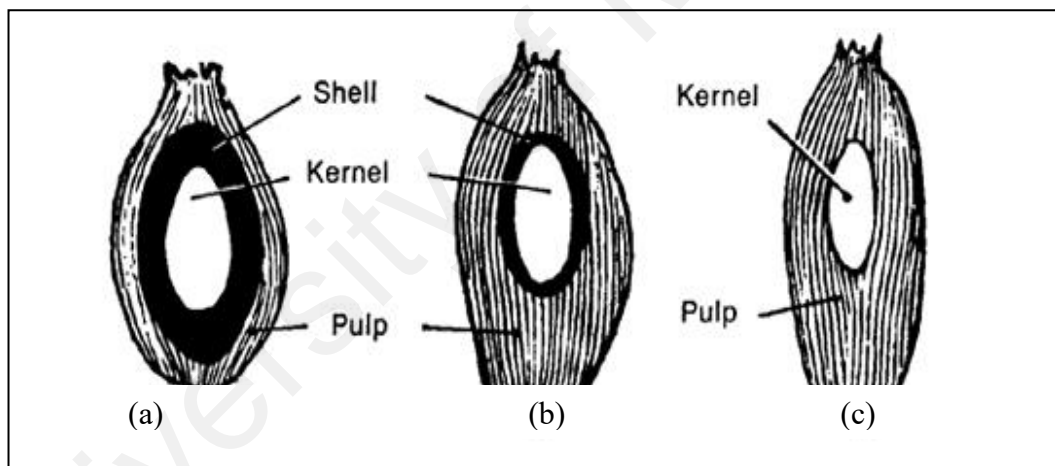


**Figure 2.2: Cross-longitudinal section of oil palm fruit varieties (a) *Dura*, (b) *Tenera* and (c) *Pisifera*, showing the relative proportions of shell, kernel and pulp**  
Source: FAO, 2002

## **2.4 Palm Oil and Palm Kernel Oil Products**

The oil palm is the highest yielding and highly profitable oil crop to many third world humid tropic countries. Oil palm is a unique crop that it produces two types of oil from its fruits, the hard-shelled nut surrounded by pulp (mesocarp) that contains the palm oil and the nut from the kernel is extracted leaving a proteinaceous residue (Corley & Tinker, 2015).

The expansion of oil palm cultivation has been much depending on the success of extracting oil and kernels from the harvested fruit punch. The palm oil has found many uses, especially 80% of it is mainly used in food such as cooking oil, shortening, and margarine. Meanwhile, the palm kernel oil has a different fatty acid structure of palm oil. It is applicable in non-edible products such as detergents and cosmetics (Aik, 2015).

## **2.5 Pests and Diseases of Oil Palm**

The real threat to declining in yields and productivity of oil palm is the presence of pests and diseases. The oil palm was free from pests and diseases attack until World War II, but as the crop area has expanded, the outbreaks of disease have been serious in several parts of the world (Corley & Tinker, 2003).

### **2.5.1 Oil Palm Pests**

Pests and organisms can damage crops by their feeding and burrowing activities that can lead to disrupting the plant physiology leading to direct cellular tissue damage and the crop's ability to optimise production (SALCRA, 2012). Four groups of pests that affecting oil palm trees: vertebrates consisting of mammals and birds; arthropods (insects and mites); mollusks, slugs, and snails; and nematodes (Verheye, 2010). In Malaysia, two major pests that attack oil palm are mammals and insects. Rat is the

major mammalian pest, meanwhile, bagworms, nettle caterpillars, termites and rhinoceros beetles are the major insect pests (Arif *et al.*, 2011).

### 2.5.2 Oil Palm Diseases

Idris (2004) listed six major diseases that attack palm trees, namely Vascular Wilt, Leaf Spot, Red Ring, Sudden Wilt, Bud and Spear Rot and Basal Stem Rot (BSR). These diseases are region-specific and attacked to certain oil palm growing areas of the world. Among the various fungal diseases affecting oil palm, BSR or *Ganoderma* disease caused by soil borne fungus *Ganoderma spp.* is the most destructive disease that causes major losses in oil palm industry with high incidence in Malaysia and Indonesia, and lower incidences recorded in Thailand, Africa and Papua New Guinea (Idris *et al.* 2004; Susanto *et al.*, 2005; Kinge & Mih, 2011).

### 2.6 *Ganoderma* Disease of Oil Palm

Fifteen *Ganoderma* fungus species have been recorded from different parts of the world (Turner, 1981). In Malaysia, three types of *Ganoderma* fungi that attack oil palm crops are *G. boninense*, *G. miniatocinctum* and *G. zonatum*. Meanwhile, *G. tornatum* does not cause disease but only live on a dead palm tree (Idris, 2004). However, *G. boninense* is the major culprit for *Ganoderma* disease attack of oil palm in Malaysia (Turner, 1981; Singh, 1991; Flood *et al.*, 2000; Idris *et al.*, 2009; Wong *et al.*, 2012).

*Ganoderma boninense* is a polyporoid fungus that belongs from the family of Ganodermataceae, order of Polyporales and Classed under Basidiomycetes (Idris, 2009). *Ganoderma* is a white rot fungus that attacks the trunk xylem tissue and leaving white cellulose through the production of enzymes that degrade the lignin components and would lead to the decay of the stem or roots from where the basidiocarps appear (Paterson, 2007; Hushiarian *et al.*, 2013; Liaghat *et al.*, 2014). *Ganoderma* is the only

pathogenic disease causing significant losses that can kill more than 80% of the oil palm stands by the time they are halfway through their normal economic life (Turner, 1981).

*Ganoderma* fungus attack starting from the root and base of the tree involving young trees and many occur on mature palm trees. Any age of palms is susceptible to *Ganoderma* attack, even younger palms between 12-24 months can be attacked by the disease. The infection becomes frequent after 4 to 5 years in replanting areas (Idris, 2004). Besides, the *Ganoderma* fungus has been found in seedlings where symptoms appear before time and critical (Sanderson, 2005; Susanto *et al.*, 2005). This occurs when the palms are felled in the process of replantation where *Ganoderma* fungus that attacks are derived from palm or coconut trees felled (Turner, 1981). The disease used to attack older palms planted on ex-coconut, but now the disease is prone to attack younger replants due to continuous replanting (some into the third cycle) (Aik, 2015).

This shows that the fungal variability is related to the capability of the species to adapt and survive in a different substrate for a long time (Chong *et al.*, 2017). Figure 2.3 shows the *Ganoderma* characterisation by their woody basidiocarps. Meanwhile, Figure 2.4 shows the basal stem rot of oil palm.



**Figure 2.3: Basidiocarps at the basal stem of oil palm**



**Figure 2.4: The rotten oil palm stem base affected by *Ganoderma* disease**

## **2.7 *Ganoderma* Symptoms and Disease Development**

Three main ways that the fungus spreads are through roots by the inoculum left by the alternative host plants, the inoculum from infected trees spreading by mycelial root contact and through airborne basidiospores. Fungi that rot and eventually kill oil palm trees may be costing and caused a decline in oil palms productivity (Hushiarian *et al.*, 2013). In general, the initiation of *Ganoderma* disease in oil palm by *G. boninense* is established from infected debris that enters and gets in contact with the roots and wounded part and progresses mainly through the cortex of the palm (Chong *et al.*, 2017). The *Ganoderma* fungus builds up along the palm infected root and after some time reaches the bole of the palm trunk (Basri *et al.*, 2003). Currently, *Ganoderma* is detected visually by finding fungal fruiting bodies (mushrooms) on the contaminated trunks (Liaghat *et al.*, 2014).

*Ganoderma* disease does not show any visible symptoms when the severity level of infection is around 8% in plant roots (Naher *et al.*, 2012). It is difficult to detect a foliar symptom of the *Ganoderma* disease as it appears in the advanced stages of the infection (Liaghat *et al.*, 2014). However, the initial symptom of *Ganoderma* disease occurs in the canopy appearance or frond wilting and malnutrition (deficiency in nitrogen) due to

restricted water and nutrient supplies to the aerial parts (Turner, 1981; Turner & Gillbanks, 2003).

In younger palms, the symptoms of *Ganoderma* disease consist of a one-sided yellowing of the lower frond and followed by necrosis (Singh, 1991). Similar symptoms also observed in mature palms, where the lower leaves collapse and hanging vertically downward from the attachment of the trunk. Furthermore, the symptoms continue with the drooping of younger leaves that turn into pale olive green or yellowish colour. This would lead the base of the stem becomes blackens, the gum may be emitted and the characteristic fructifications of basidiocarps appear. In severe cases, the whole crown may then fall off, or the trunk may collapse (Corley & Tinker, 2003).

Mature palms can survive up to 3 years while young palms die within 1 or 2 years after being diagnosed with the disease (Corley & Tinker, 2003). Two types for the confirmation of *Ganoderma* disease diagnostic symptoms include the observation of the disease at the palm base and the appearance of one or more fruiting bodies (Gait, 2012).

## **2.8 Control and Treatment of *Ganoderma* Disease**

Vegetative growth and production not only determine the oil palm yields but also by the approach to control and eradicate pests and diseases (Verheyne, 2010). Cultural and chemical control methods have proved to be ineffective towards the disease. Meanwhile, diagnosis and prevention of *Ganoderma* disease have proved difficult. However, it is convenient to deal with the stage of the disease severity at which the palm is affected (Corley & Tinker, 2003). These include a surgical method to control *Ganoderma* on sick palms by removing the infected stem and root tissue at the base of the plant. However, this method is less effective since *Ganoderma* can grow back a few months after the treatment. Another method to control the infected *Ganoderma* is through soil mounding. This method includes filling in around palm with a land area of 1 meter high



and 0.75 meters wide on palms that are 10 years and older. This method does not fully kill the *Ganoderma*, but it has been reported to extend the age of the infected palms (Idris, 2004).

Visual interpretation in detecting *Ganoderma* disease is time-consuming since the disease can only be detected at the middle or late stages of the disease. With decades of research on *Ganoderma* disease, there have been several bio-controls and fungicides developed and produced by Malaysia Palm Oil Board (MPOB) for control and management of the disease (Idris *et al.*, 2012; Idris *et al.*, 2014a; Idris *et al.*, 2014b). The technologies include *Ganoderma* Selective Medium (GSM) (Ariffin *et al.*, 1993), Polyclonal Antibodies Enzyme-Linked Immunosorbent Assay (PABs-ELISA) (Idris & Rafidah, 2008; Madihah *et al.*, 2014), Multiplex PCR-DNA Kit (Idris *et al.*, 2010a) and GanoSken Tomography (Idris *et al.*, 2010b). However, these technologies are disfavoured since it requires a lot of labour intensive, time-consuming and costly (Izzuddin *et al.*, 2015).

Hence, remote sensing technology has the potential to assist in monitoring huge oil palm plantation and have the possibility to detect *Ganoderma* disease in oil palm. The recent development of remote sensing technology is the unmanned aerial vehicle (UAV) that gives more flexibility and higher quality of data and can be set to obtain images that independent from cloud cover (Klemas, 2015). Figure 2.5 shows the simplified of several technologies used for *Ganoderma* disease detection developed by MPOB.

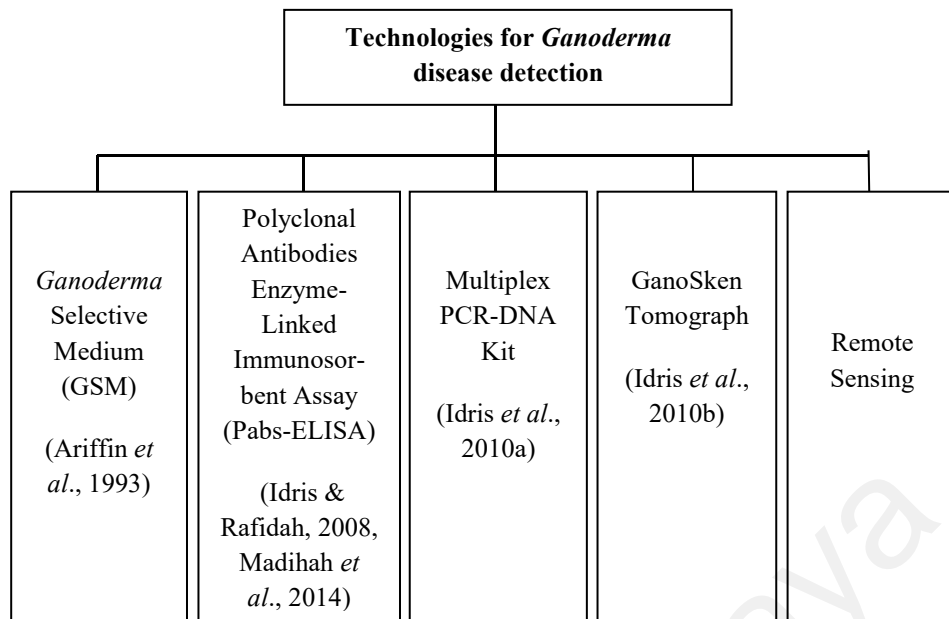


**Figure 2.5: Technologies developed by MPOB for *Ganoderma* disease detection**

## 2.9 Remote Sensing Principles

Remote sensing is the science of collecting and interpreting information of an object by acquiring data with a device, not in contact with the object (Lillesand *et al.*, 2014). In general, remote sensing using electromagnetic (EM) radiation with the sun being an ultimate source. Every physical object absorbs and reflects EM radiation. Each object has a different surface features that generate a different absorption or reflection from the sun's radiation (Smith, 2012).

## 2.10 The Electromagnetic Spectrum

Electromagnetic (EM) radiation appears as a continuation of wavelengths and frequencies, and the entire range of EM radiation is called the electromagnetic spectrum. The wide range of wavelengths going from the shortest wavelength (gamma rays) to long wave microwaves (Curran, 1985; Joseph, 2005). The most common EM spectrum in remote sensing sensors on Earth observation is visible, infrared and microwave (Chuvieco & Huete, 2010; Duzgun, 2011).

The wavelengths that normally used in remote sensing are visible and near infrared radiation in the waveband 0.4-3 $\mu$ m, visible spectrum in the waveband 0.4-0.7 $\mu$ m, infrared radiation in the waveband 3-14 $\mu$ m and microwave radiation in the waveband 5-500mm (Curran, 1985; Joseph, 2005). Figure 2.6 shows the variations of different EM spectrum.

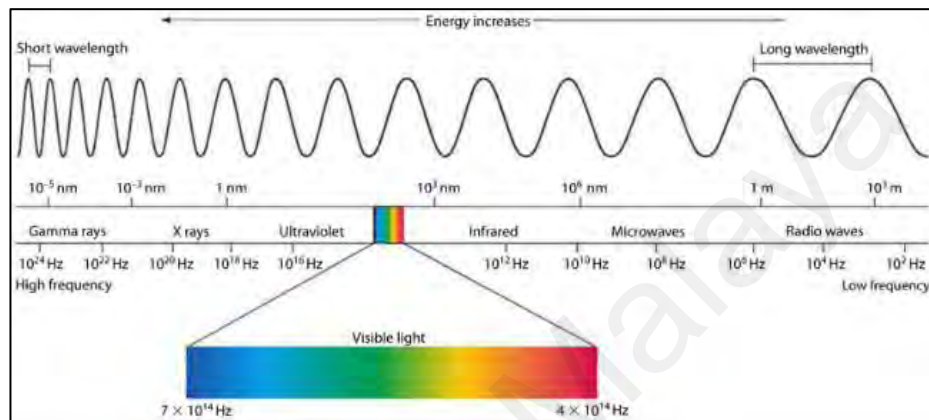


**Figure 2.6: Electromagnetic spectrum, with shortwave energy depicted to the left and long wave to the right**  
**Source: Purkis & Klemas, 2011**

## 2.11 Remote Sensing Sensors

Through a different range of the electromagnetic spectrum, sensors can be classified depends on the measuring range (visible=VIS, near infrared=NIR, short wave infrared=SWIR, thermal infrared=TIR), the measuring scale (near-range or remote), and into imaging and non-imaging sensors (Mahlein *et al.*, 2012). An ideal sensor would be spatially detailed data that are highly sensitive to all wavelengths throughout the spectrum across wide areas on the ground (Lillesand *et al.*, 2014). The sensor can operate from any type of platform or vehicle that range from step ladders to aircraft (fixed-wing or helicopters) and to satellites.

Two types of remote sensing sensors are active and passive. An active sensor requires an external source of radiation to emit energy to the object and scan the backscattered radiation (Kapilevich *et al.*, 2014; Maryam *et al.*, 2016). An example of the remotely sensed sensor is radio detection and ranging (RADAR) which transfer a microwave signal to the target, detects and determines the backscattered portion of the signal. Besides that, light detection and ranging (LiDAR) is another example that gives off a laser pulse and precisely measures its return time to calculate the target height. Active sensors can be used to image the target or surface at any time, any season, day or night (Wang & Weng, 2013).

Passive sensor measure levels of energy that are naturally emitted, reflected or transmitted by the target object from the sun which is the source of radioactive energy. Data can only be captured during daylight hours since passive sensor uses naturally occurring energy. The sun's energy is reflected for visible wavelengths and re-emitted for thermal infrared wavelengths. (Gopi *et al.*, 2014). Examples of passive sensors are multispectral and hyperspectral sensors such as photographic cameras and thermal IR sensors (Jensen 2006; Wang & Weng, 2013).

## **2.12 Multispectral Remote Sensing**

Multispectral sensors mounted on the satellite or aerial platforms were used to capture remotely sensed data. Recent years have seen the conversion from film-based sensors to digital sensors, which result in very high resolution remotely sensed data. The multispectral image can be expressed in three dimensions: (1) spatial, (2) spectral and (3) temporal (Navulur, 2006).

### 2.12.1 Spatial, Spectral and Temporal Characteristics

Spatial resolution, spectral coverage and temporal frequencies are the main attributes and the fundamental basis of remote sensing systems for gathering information remotely (Landgrebe, 2005). Spatial resolution describes the sharpness of spatial detail, or the smallest size of the object that can be resolved by the sensor represented by pixels (Purkis & Klemas, 2011).

Spectral coverage refers to the spectral band number, a measurement of the specific wavelength spectrum of different colours and parts that a sensor can record (Navulur, 2006; Purkis & Klemas, 2011). The images from sensor differ according to the spectral bandwidth of energy captured by the image ranging from panchromatic to hyperspectral (Entwisle & Stern, 2005). The most common sensors used in agriculture is the multispectral sensors that have less than ten bands, superspectral sensors have more than ten bands and hyperspectral sensors that have bands in the hundreds.

Temporal frequency refers to the cycle or constellations of coverage, or how often the same area is visited by the sensor and describes a series of images that captured by the same sensor over time (Chuvieco *et al.*, 2010; Purkis & Klemas, 2011). It is vital to use images that have high spectral and temporal resolution; from satellite and aerial systems to generate remote sensing product (Mesas-Carrascosa *et al.*, 2014).

### 2.13 Multispectral Image Analysis

The spectral responses of various characteristics in different spectral bands are known as multispectral image analysis techniques. Dissimilar spectral responses in various bands are different according to its features (Navulur, 2006). Figure 2.7 shows the graph of the reflectance of water, soil and vegetation in different wavelengths. The

greater the reflectance in the visible range, the brighter the type of objects looks at an image.

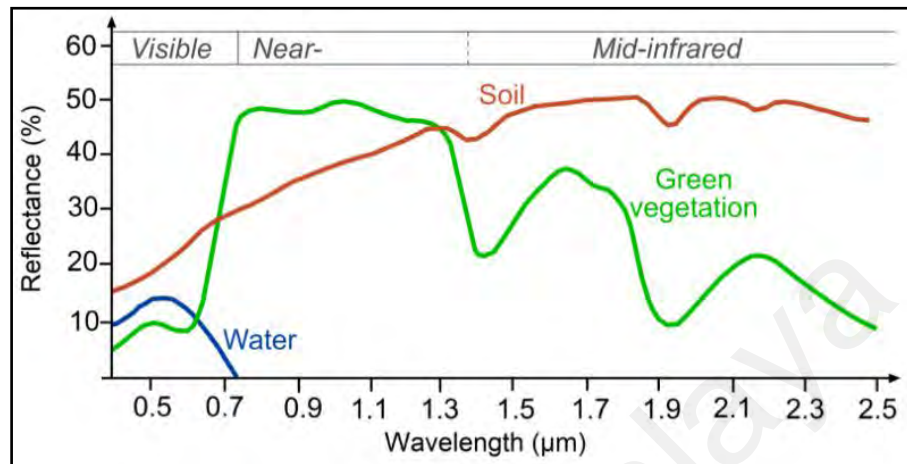


**Figure 2.7: Reflectance of water, soil and vegetation in different wavelengths**  
Source: Navulur, 2006

#### 2.14 Remote Sensing Platforms

Platforms are the base on which remote sensing instruments or sensors are placed to view and image targets on Earth's surface (Kumar, 2005). There are three main methods of collecting remotely sensed images, from satellite and aircraft platforms, and recently the unmanned aerial vehicle (UAV) platform. Each platform has pros and cons that involve operational, technological and economic factors (Matese *et al.*, 2015).

Satellite platforms can survey large areas at the same time. However, the image taken may suffer from cloud cover and have a coarse resolution. Meanwhile, aircraft platforms are more flexible but are too costly and difficult (Matese *et al.*, 2015). In recent years, the UAV has become an increasingly important platform for remote sensing data acquisition (Lillesand *et al.*, 2014).

Low altitude remote sensing (LARS) system is one of among other remote sensing platforms and used as one of the favourable platforms for precision farming and monitoring crops for agricultural applications (Saberioon *et al.*, 2014). UAV being the LARS system provides a small-scale platform for research applications, but somehow its limited payload and short flight endurance are its weaknesses (Matese, 2015). Table 2.3 shows the comparison between UAV with airborne and satellite platforms.

**Table 2.2: Comparison of UAV with manned airborne and satellite platforms**

<i>Platform</i>	<i>Spatial Resolution</i>	<i>Field of View</i>	<i>Usability</i>	<i>Payload Mass</i>	<i>Cost for Data Acquisition</i>
UAV	0.5-10 cm	50-500 m	Very good/ easy	Can be limited	Low
Helicopter	5-50 cm	0.2-2 km	Pilot mandatory	Almost unlimited	Medium
Airborne	0.1-2 m	0.5-5 km	Pilot mandatory	Unlimited	High
Satellite	1-25 m	10-50 km	-	-	Very high

**Source: Candiago *et al.*, 2015**

### 2.15 Unmanned Aerial Vehicle (UAV)

Unmanned aerial vehicle (UAV) or drones are remotely piloted light aircraft that can carry sensors or cameras in support of remote sensing applications (Campbell & Wynne, 2011). The UAV is one of the methods used to collect data from the remote area since it has flexibility along with high spatial and temporal resolution (Pan *et al.*, 2011). The UAV is remotely controlled by wireless signals from the ground or operated by its own program.

Currently, there are three types of UAV platforms that are widely used: fixed-wing, multi-rotor, and single-rotor UAVs. Single-rotor (similar structure to a helicopter) UAVs have efficient power consumption. Compared to single-rotor UAVs, multi-rotor UAVs has the capability to take off and land vertically. Meanwhile, a fixed-wing UAVs consist of a rigid wing frame that has a fixed airfoil that makes flight capable by the

UAV's forward airspeed that causes generating lift. The airspeed is a forward thrust that is generated by the means of a propeller being turned by an electric motor (QuestUAV, 2015, Jayathunga *et al.*, 2018).

Several advantages of UAV over piloted aircraft and satellites are they are safer and less costly than piloted aircraft; flexible and easy to deploy (Rango *et al.*, 2009). The main components of a UAV consist of sensor payloads for data acquisition, autopilot to control the entire craft, the global positioning system (GPS) for navigation and ground station for mission planning (Klema, 2015; Feng *et al.*, 2015). The UAV is capable to collect multispectral image at cm-level resolution when coupled with imaging, ranging and positioning sensors (Candiago *et al.*, 2015).

Due to tropical regions, especially in Malaysia that experience significant cloud cover, the quality of data collected from satellite and airborne platforms is sometimes unpredictable. Therefore, UAV platform represents a low-cost remote sensing that provides cost-effective data product that is free from cloud cover and as an alternative to airborne and satellite platforms (Jayathunga *et al.*, 2018).

## **2.16 Plant Signal Interaction**

Near-range remote sensing provides high possible techniques in detecting infected plants with diseases and monitoring crops strands. The EM radiation and interaction with plant or soil material plays an important part for remote sensing application. Remote sensing measures the reflected radiation, rather than transmitted or absorbed radiation (Mulla, 2013). The living leaf chlorophyll or plant pigments absorb blue and red light for photosynthesis (Figure 2.8). They absorb much less of green light and more is reflected from the visible spectrum, so the human observer can see the dominant reflection of green light as a healthy vegetation. Meanwhile, the near infrared spectrum leaf reflectance is controlled by the structure of the spongy mesophyll tissue. The



radiation that passes through the upper epidermis is strongly distributed by mesophyll tissue within the leaf (Campbell & Wynne, 2011).

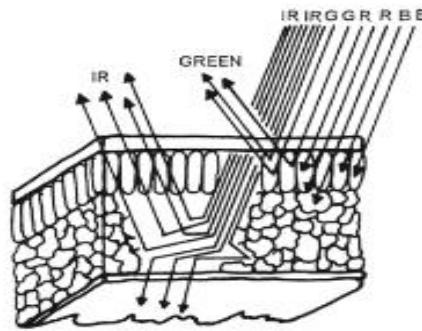


**Figure 2.8: The interaction of leaf structure with visible and infrared radiation.  
Red and blue absorbed largely for photosynthesis  
Source: Campbell & Wynne, 2011**

## 2.17 Vegetation Properties

The difference between stress and healthy crops can be detected from the reflection of various wavelengths. In stressing crops, chlorophyll starts to break down and this will affect the cellular structure of the leaves. The chlorophyll loss will affect the crop reflectance in the visible and NIR region. The changes in the NIR region that are invisible to human eyes can be identified using remote sensing before the chlorotic symptoms appear (Muhammad *et al.*, 2015).

Leaf reflectance can be described as the proportion of the illuminated light reflected by the leaf. The common features of the reflected spectrum present in healthy plants consist of low reflectance at visible wavelengths (RGB = 400-700 nm) due to the strong absorption of the photo-active pigments, and high reflectance in the near-infrared (NIR = 700-1200 nm) in which there is the strongest interaction with the tissue of the leaf (Tona, 2017).

## 2.18 Remote Sensing for Precision Agriculture

Precision agriculture is the trend of agricultural development of the world. The traditional precision agriculture focuses on three systems (Remote Sensing, Geographic Information System, and Global Position System) for decision-supported technologies in crop production management (Yue *et al.*, 2012). An added advantage of remote sensing is that it can look at a wide area and make a comparison between healthy and stressed crop data at the same time (Venkateswarlu *et al.*, 2011). At present, precision agriculture focuses on the development of sensors using remote sensing that can remotely detect in real-time of the crop and soil properties (Schellberg *et al.*, 2008).

Hyperspectral imaging sensors or imaging spectroscopy is more complicated compared to multispectral data. This is due to the hyperspectral system collect hundreds of continuous narrow bands of the electromagnetic spectrum and lead to complex processing after the collection of data is required (Qi *et al.*, 2016; Heaphy *et al.*, 2017).

One of the uses of remote sensing technology pioneer demonstrations in agriculture was reported in a plantation crop. The ability to detect stresses detail in oil palm plantations has increased as remote sensing technologies have evolved. Several kinds of research of remote sensing for *Ganoderma* disease detection have been developed by MPOB. A few techniques of hyperspectral remote sensing have been examined for *Ganoderma* disease detection using handheld spectroradiometer (Shafri & Izzuddin, 2008; Nisfariza *et al.*, 2010; Shafri *et al.*, 2011; Izzuddin *et al.*, 2015) and using hyperspectral imaging attached to an airborne platform (Nisfariza, 2012; Shafri *et al.*, 2012; Izzuddin *et al.*, 2013).

## **2.20 Application of Remotely Sensed Sensors in *Ganoderma* Disease Identification**

### **2.20.1 Hyperspectral Remote Sensing in *Ganoderma* Disease Detection**

Several remotely sensed methods have been used for *Ganoderma* disease identification and it is severity categories that comprise of hyperspectral remote sensing, multispectral remote sensing, terrestrial laser scanning, tomography, Intelligent Electronic Nose, micro-focus X-ray Fluorescence and spatial maps (Maryam *et al.*, 2016). Only hyperspectral and multispectral remotely sensed techniques applied in *Ganoderma* disease detection will be reviewed. Table 2.4 shows the summary of remotely sensed sensors and methods applied for *Ganoderma* disease detection in oil palm.

Geophysical and Environmental Research Corporation (GER1500) handheld spectroradiometer was used in *Ganoderma* disease detection and classification. Nisfariza (2010) studied the relationship of *Ganoderma* disease attack towards oil palm leaves reflectance spectra using the continuum removal index. The study classified between young palm age of 5 years old and matures palm age of 17 years old using three different groups that are T1 (healthy palm), T2 (*Ganoderma* infected palm without foliar symptom, but with white mycelium at stem base) and T3 (*Ganoderma* infected palm with foliar symptoms and white mycelium at the stem base). Three continuum removed zones located in blue (400-550 nm), red (550-750 nm) and near-infrared (915-970 nm) regions were selected. The results could separate severity levels of T1 and T2, and T1 and T3. However, it could not separate between T2 and T3.

The efficiency of Airborne Imaging Spectrometer for Applications (AISA) was tested for assessing and mapping *Ganoderma* disease infecting oil palm. Shafri *et al.* (2012) applied the best AISA hyperspectral indices in mapping stressed oil palm trees using vegetation indices and red edge techniques. Two AISA wavelength bands were

selected at locations of 616 nm (red) and 734 nm (NIR) were based on laboratory statistical analysis using field spectroradiometer reflectance data. Three new formulated hyperspectral indices, namely D2, normalized difference vegetation index an (NDVIa) and transformed vegetation index a (TVIa) were applied on these two bands. The image index was then applied using the Spectral Angle Mapper (SAM) and minimum distance classifiers to classify the palms into two classes of infected and non-infected. The classification results were evaluated using the confusion matrix and compared to SAM. The overall accuracy proved that D2 and NDVIa acquired the highest accuracy of 86%, followed by TVIa with 84% overall accuracy.

Izzuddin *et al.* (2017) presented the outcome of using APOGEE spectroradiometer to develop spectral indices of oil palm seedlings from three levels of *Ganoderma* disease severity where T1 is healthy palm, T2 is mild infected palm and T3 is severely infected palm. The analysis involved spectral indices and total leaf chlorophyll (TLC) using a regression technique. The results showed that among the six spectral indices used, Ratio 3 is the best spectral index for the early detection of *Ganoderma* infection in oil palm seedlings.

### **2.20.2 Multispectral Remote Sensing in *Ganoderma* Disease Detection**

Unlike hyperspectral sensors, multispectral systems capture the reflected or emitted of a few broad wavelength bands inbound from the Earth's surface across the electromagnetic spectrum (Qi *et al.*, 2016).

Santoso *et al.* (2011) proved the identification of *Ganoderma* disease in oil palm using ground truth data by showing higher reflectance in RGB and lower reflectance in NIR electromagnetic regions using QuickBird high-resolution satellite image. Six different vegetation indices were used to discriminate intact palms from infected ones, namely Atmospherically Resistant Vegetation Index (ARVI), Green Normalized

Difference Vegetation Index (GNDVI), Green Blue Normalized Difference Vegetation Index (GBNDVI), Normalized Vegetation Index (NDVI), Soil Adjusted Vegetation Index (SAVI) and Simple Ratio (SR). GNDVI and GBNDVI were identified to provide good results in assessing infection rates of 10 years old palms. Meanwhile, ARVI and SR indices showed the most accurate in 16 years old palms. Besides, the satellite multispectral image analysis showed two patterns of disease propagation that are dendritic (in the younger palm with medium to low infection) and sporadic (in older palms) patterns. The mapping accuracy is 84% of image partitioning that effectively presented areas that were infected by the disease.

The identification between healthy and *Ganoderma* infected oil palm can be classified using colour indices using multispectral and thermal cameras. Khairunniza-Bejo *et al.* (2015) used thirteen colour indices consist of normalized difference vegetation index (NDVI), red (R), green (G), blue (B), near-infrared (NIR), green-blue (GB), green/blue (G/B), green-red (GR), green/red (G/R), hue (H), saturation (S), intensity (I) and thermal index (T) to analyse the healthiest level of oil palm using 216 fronds sample. Three fronds with frond number 1, 9 and 17 were taken from each palm. From the analysis, it can be concluded that G is the best colour index to distinguish between healthy and *Ganoderma* infected palm, where healthy palm has a greater index as compared to the infected palm. Besides, G band also shows greater average value compared to R and B bands due to chlorophyll pigment takes in the most energy.

## **2.21 UAV-Based Platform in Oil Palm Monitoring**

The development of low-cost digital camera is more on visible and near-infrared colours. Images can be easily taken from the camera and transfer to the computer for processing and analysis. The rapid increase of UAV technology benefits the crop management; particularly for studying crop as well as the detection and mapping of

plant stress (Calderón *et al.*, 2012; Garcia-Ruiz *et al.*, 2013), plant monitoring (Bulanon *et al.*, 2014; Chaves *et al.*, 2015) and crop maturity (Saberioon *et al.*, 2014).

Despite the potential of UAVs in precision agriculture applications, very few studies have included detailed analyses of UAV photogrammetric products over oil palm areas. UAV application in oil palm has been widely applied for oil palm tree counting (Mansur *et al.*, 2014; Takeuchi & Khiabani, 2017) and for oil palm monitoring (Astina *et al.*, 2015; Fahmi *et al.*, 2018) using UAV multispectral images.

Mansur *et al.* (2014) deployed the use of UAV imagery with visible and near-infrared bands for automated oil palm tree counting. Convolution and morphological analysis from spatial analysis was used to detect and delineates the oil palm crown. To create the oil palm centroids, image thresholding was used. The result was assessed by comparing with ground truth and it was proved that the result accuracy is 96.5% accurate.

Meanwhile, Astina *et al.* (2015) presented the outcome of the spectral response curve of oil palm tree growth using UAV platform with three spectrums of RGB and single spectrum of NIR. A spectral response curve graph was able to determine the growth of the oil palm trees using Normalized Difference Vegetation Index (NDVI) and Modified Soil-Adjusted Vegetation Index 2 (MSAVI2) using the UAV orthophoto images. The spectral reflectance graph was generated to identify or detect the level of the condition of the trees based on the value of the index range. The study has been proved to generate a good spectral response curve for oil palm after comparing with ground-based spectroradiometer observation.

Hyperspectral development integrated with UAV resulting in smaller and lighter sensor gives the ability for measuring hundreds of bands that are more useful towards agricultural crops especially in oil palm plantation (Adão *et al.*, 2017). However, there is a lack in using UAV hyperspectral image in oil palm plantation.

Previous multispectral research of remote sensing in oil palm mainly address utilisation of satellite and imageries on general mapping of oil palm plantation. Based on the literature review, there are no previous study that addressed the utilisation of UAV for *Ganoderma* disease. A number of studies used UAV for mapping and tree counting for plantation management purposes. This study would close the research gap on the potential of UAV for *Ganoderma* disease detection, although the number of bands are limited as compared to the multispectral imageries on satellite. The improvements were significant to the pixel size and spatial resolution which is useful for features extraction in future studies.

**Table 2.3: Summary of remotely sensed sensors and methods used in oil palm studies**

<i>Remotely Sensed Technique</i>	<i>Sensor Platform</i>	<i>Applied Sensor</i>	<i>Sensor Characteristics</i>		<i>Applied Methods</i>	<i>References</i>
			<i>Spectral Range</i>	<i>Spectral Resolution</i>		
<i>Hyperspectral</i>	Ground-based	GER 1500 handheld spectroradiometer	350-1050 nm	3.2 nm	Continuum Removal Index	Nisfariza (2010)
		APOGEE spectroradiometer	350-1000 nm	0.5 nm	Total Leaf Chlorophyll	Izzuddin <i>et al.</i> (2017)
	Airborne	AISA sensor	430-900 nm	6.43 nm	Minimum Distance Classifier and Spectral Angle Mapper	Shafri <i>et al.</i> (2012)
<i>Multispectral</i>	Spaceborne	Quickbird	450-520 nm 520-600 nm 630-690 nm 760-900 nm	1 Blue 1 Green 1 Red 1 NIR	Vegetation Index	Santoso <i>et al.</i> (2011)
	Ground-based	Condor5 VNN-285	590-670 nm 500-590 nm 400-500 nm 670-830 nm 830-1000 nm	1 Blue 1 Green 1 Red 2 NIR	Color Indices	Khairunniza-Bejo <i>et al.</i> (2015)
	UAV-based	Tetracam ADC sensor	520-920 nm	1 Green 1 Red 1 NIR	Automated Oil Palm Tree Counting	Mansur <i>et al.</i> (2014)
		Canon powershot XS260 camera	450-900 nm	1 Blue 1 Green 1 Red 1 NIR	Normalized Difference Vegetation Index and Modified Soil-Adjusted Vegetation Index 2	Astina <i>et al.</i> (2015)



## CHAPTER 3: METHODOLOGY

### 3.1 Study Area

The study location is at an oil palm plantation in Seberang Perak, in the district of Seberang Perak, Perak, Malaysia (Figure 3.1). The study area is located between 4° 6' 42" N latitude and 100° 53' 12" E longitude with annual precipitation of 2256 mm per year and temperature between 24°C - 34°C. The area consists of 8 years old *dura* × *pisifera* (D×P) oil palms planted in 25 hectares (ha) planting plot. The planting plot is the first generation of oil palm plantation that previously cleared from the forest area. The topography of the area is flat, undulated with good drainage and adequate sources of water supply due to the availability of agricultural canals developed by the authorities for other agriculture nearby the study area.

The plot was selected based on several Malaysian Palm Oil Board (MPOB) censuses with the availability of ground truth census of *Ganoderma* incidences reported carried on in the year 2013 and 2014. The selected oil palm plantation is well maintained, and the area is only reported with incidences of *Ganoderma* disease with no other pests, diseases, water stress and nutrient stress. Figure 3.2 shows the overall flow chart of the study methodology and steps performed in this study that will be discussed thoroughly.

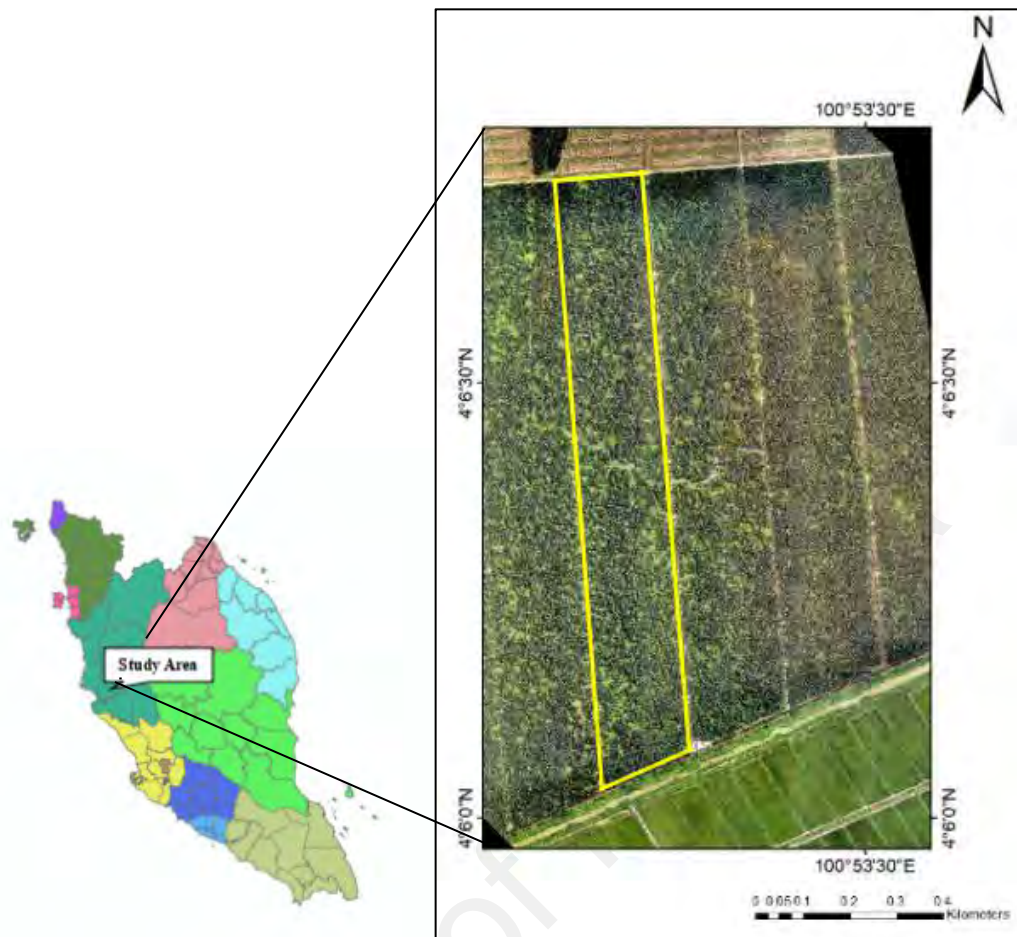


**Figure 3.1: The study site location in yellow polygon**

### **3.2 Ground Data Collection**

The ground data collection was conducted to record the number and location of healthy and infected oil palm standings in the study area. A field survey was carried out on 9-12 June 2014 in the plot to assess the accuracy of the red-green-blue (RGB) and near-infrared (NIR) images and image processing procedures. The ground data collection was conducted to assist the orthophoto image classification. Data collected on the ground consisted of the *Ganoderma* disease census of each individual palm in the study area and coordinate sampling of several distinguishing marks in the areas for geometric correction of airborne images. There are 3,041 palm trees on the plot and the health status of each healthy and infected palms was observed manually and evaluated.

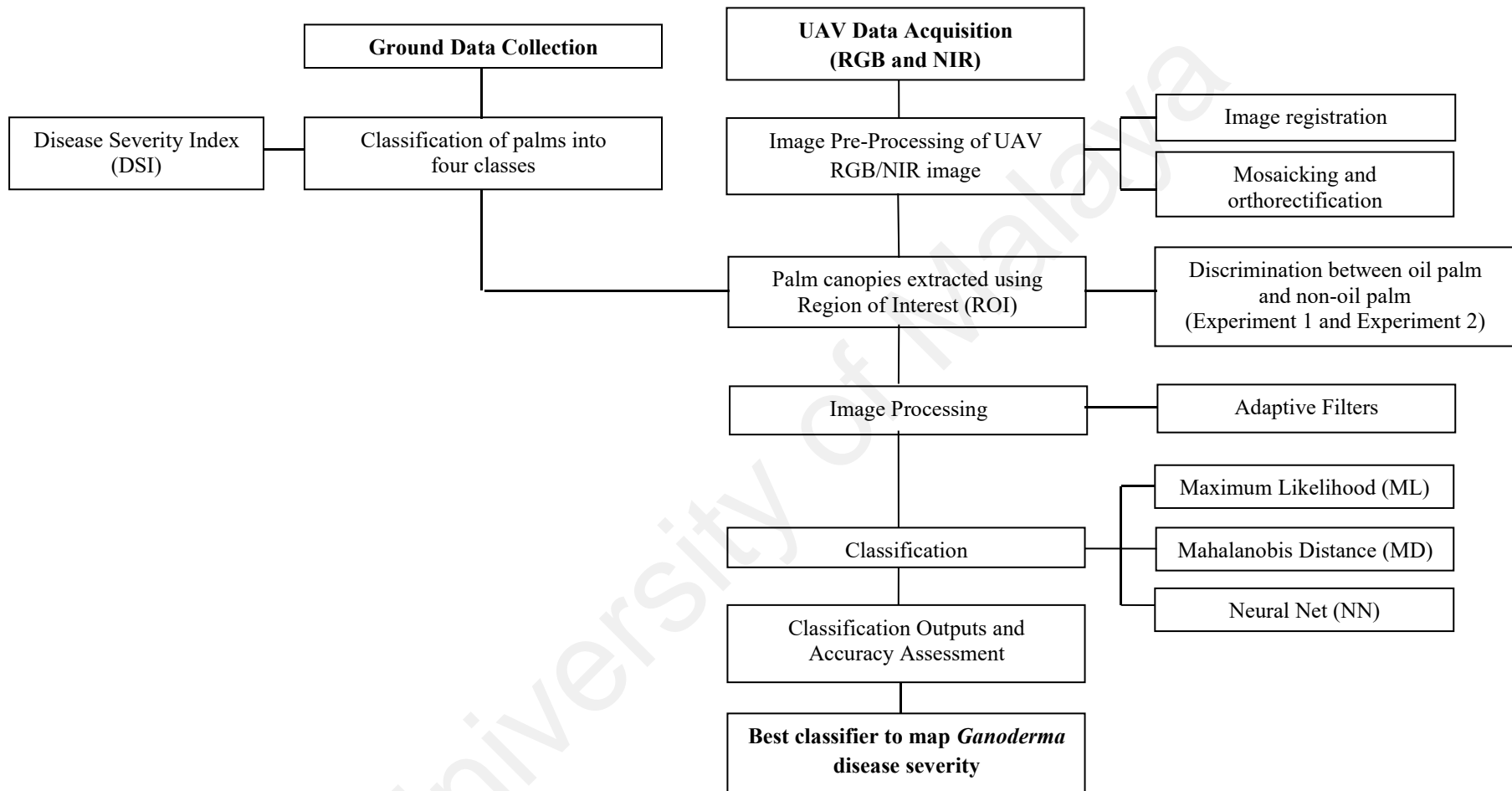






**Figure 3.2: The overall flow chart of the methodology**

### 3.3 Classification of Treatments

The census and visual assessment were conducted by the technical staff of *Ganoderma* and Diseases Research for Oil Palm (GANODROP) Unit, Biological Research Division, Malaysian Palm Oil Board (MPOB) under the supervision of Dr. Idris Abu Seman (Head, GANODROP Unit). There are two different experiments conducted in this study.

For Experiment 1, the oil palm was categorised into four categories of Disease Severity Index (DSI) of *Ganoderma* disease for classification of treatments which are healthy (T0), mild symptom (T1), moderate symptom (T2) and severe symptom (T3). Figure 3.3 shows the infected oil palms that were categorized into four classes of DSI in Experiment 1. Meanwhile, Table 3.1 shows the DSI and the description of the visual symptoms for Experiment 1. The DSI was determined based on the *Ganoderma* disease severity categories that have been standardised by the Malaysian Palm Oil Board (MPOB). The palms were selected and categorised based on the visual assessment of the palm foliar characteristics and the appearance of *Ganoderma boninense* basidiocarp at the stem base of the palm. The total number of T0 is 2513, T1 is 227, T2 is 146 and T3 is 155.

<b>T0</b> <b>Healthy palm</b>	<b>T1</b> <b>Mild infected palm</b>	<b>T2</b> <b>Moderate infected palm</b>	<b>T3</b> <b>Severe infected palm</b>
Canopy looks healthy, no presence of <i>Ganoderma</i> fruiting body	Canopy looks healthy, presence of <i>Ganoderma</i> fruiting bodies or stem rotting	Canopy yellowing and wilting (<50%), presence of <i>Ganoderma</i> fruiting bodies and stem rotting (<30%)	Canopy yellowing and wilting (>50%), presence of <i>Ganoderma</i> fruiting bodies and stem rotting (>30%)
			

**Figure 3.3: Four classes of DSI that infected the oil palms**

**Table 3.1: *Ganoderma* Disease Severity Index (DSI) and visual symptoms for Experiment 1**

<i>DSI</i>	<i>Category</i>	<i>Visual Symptoms</i>
T0	Healthy palm	No fruiting body, foliar symptom and stem rotting.
T1	Mild infected palm	Presence of white mycelium or fruiting body (eg: small white button form). No foliar symptoms and slightly or no stem rotting (<10%) at the base.
T2	Moderate infected palm	Presence of white mycelium or fruiting body (eg: small white button or bracket shape form). Palm shows foliar symptoms (<50%) and slightly stem rotting (<30%) at the base
T3	Severe infected palm	Presence of white mycelium or fruiting body (eg: small white button or bracket shape form). Palm shows severely foliar symptoms (>50%) and stem rotting (>30%) at the base.

Meanwhile, Table 3.2 showed the description of another *Ganoderma* DSI in Experiment 2 which was normally used by commercial plantation managers in the visual detection of *Ganoderma* disease. There are two categories in Experiment 2 where the healthy category is a T0 from Experiment 1 DSI; meanwhile, the unhealthy category is a combination of T1, T2, and T3 from Experiment 1 DSI. There is a very minute difference between healthy and unhealthy categories and that is why it is regrouping in one category.

**Table 3.2: *Ganoderma* Disease Severity Index (DSI) and visual symptoms for Experiment 2**

<i>Category</i>	<i>Visual Symptoms</i>
Healthy	Canopy and leaves look healthy, no presence of <i>Ganoderma</i> white mycelium, small white button, fruiting bodies or rotting at the palm base.
Unhealthy	Presence of leaves yellowing, fronds wilting, two or three unopened spears and presence of <i>Ganoderma</i> white mycelium, small white button, fruiting bodies or rotting at the palm base.

### 3.4 Flight Mission

#### 3.4.1 Platform

This study used a Swinglet CAM (Figure 3.4), which is a fixed-wing unmanned aerial vehicle (UAV), manufactured by Sensefly, a Parrot Company, Switzerland. The specification of the UAV Swinglet is shown in Table 3.3. The images were acquired on 11 June 2014, capturing the overhead perspective of the selected oil palm plantation. The UAVs carries the camera, GPS and an inertial measuring unit (IMU) that trails the position of the UAV and enable autonomous flight system.



**Figure 3.4: Swinglet with modified compact camera**

**Table 3.3: Specification of UAV Swinglet**

Weight	0.5 kg
Wingspan	80 cm
Material	EPP foam, carbon structure and composite parts
Propulsion	Electric pusher propeller, 100 W brushless DC motors
Battery	11.1 V, 1350 mAh

### 3.4.2 Sensor

The sensor used in this study was a lightweight Canon IXUS 220HS compact camera (Figure 3.5) with high resolution and wide-angle capability. The camera has been modified with NIR capability. One camera acquires the digital image in RGB and the second camera acquires the image in NIR bands. The image acquisition settings were set to have 60% overlap between each image snapshot and 30% overlap between each flight path in order to generate Digital Terrain Model (DTM) that must be used to produce an orthophoto mosaic of the RGB and NIR images. This camera could be easily mounted on the Swinglet. The camera features an effective resolution of 12.1 mega pixels and it can take photos with  $4000 \times 3000$  pixels as maximum resolution. Table 3.4 shows the technical specifications of the sensor.



**Figure 3.5: Canon IXUS 220HS camera mounted on Swinglet UAV**

**Table 3.4: Canon IXUS 220HS technical specifications**

Minimum focal length	4.3 mm
Image sensor dimensions	$6.16 \times 4.62$ mm
Sensor resolution	$4011 \times 3016$
Format	JPEG



The spatial resolution for both RGB and NIR images are 4 cm and 10 cm ground sampling distance (GSD) respectively, with a flight altitude of 150 m above ground. Meanwhile, the RGB image bands are in between 400-750 nm with red as band 1, green as band 2 and blue as band 3, and for NIR image bands are in between 760-960 nm with red as band 1, green as band 2 and NIR as band 3.

Sunlight is one of the main factors for good image data acquisition; the flight configuration was carried out in a clear sky condition. The images were acquired by performing two separate flights since it is not possible to put all sensors simultaneously on board due to the limited payload of the Swinglet. The first flight was capturing data at 13.00 and the second one around 13.30.

The flight duration has been never more than 20 minutes since the battery limitations only up to 30 minutes, along with a normal cruise speed during image acquisition about 36 km/h. The system also included automatic 3-dimensional flight planning. The software for data processing is Postflight Terra LT.

The Swinglet flew autonomously in the testing area via automatic pilot function as the control unit received coordinate input on the flight path. The operator remotely controlled the take-off and the landing. The control unit provides a monitor that consist of the flight status including battery level, signal quality, wind speed and other information.

### **3.4.3 GPS Equipment**

A Garmin Global Position System (GPS) was used before employment to put the coordinate of the selected area (Figure 3.6). The coordinate will lead Swinglet to its flight path. Swinglet were able to fly autonomously with the aid of GPS receiver and its waypoint. The GPS coordinates will help to locate and to align the images taken using photogrammetry software.



**Figure 3.6: The Garmin GPS equipment**

### **3.5 Flight Planning**

A careful flight planning needs to be conducted to obtain an excellent quality of the image data. The Swinglet flew after the preparation phase of the flight configurations. A mapping waypoint of aerial image acquisition is the key success in getting usable results. An optimized mapping waypoint will enhance the mission routing and reduce post processing computation load (Abu Sari *et al.*, 2018). In this study, the eMotion software was used to display the ground station that provides information about location, altitude, warnings and other relevant data about the UAV. Figure 3.7 shows the flight lines in eMotion software that are useful to determine the needed number of images to be captured based on the plan in flight planning software according to the time interval.



**Figure 3.7: Flight lines for Swinglet UAV**

### **3.6 Image Pre-Processing**

There are 98 snapshots of raw digital images for each RGB and NIR that was acquired by the UAV over the study plot. The images were tagged with ground coordinates from GPS and also the flight information from the Inertial Measurement Unit (IMU) system during flight. These data are important for the pre-processing of the RGB and NIR raw images to generate an orthophoto image mosaic of the study area.

There were a few essential steps in image pre-processing. The first step was to download data from the camera. The second step was to calibrate raw multispectral images. Lastly, the aerial images were mosaicked and geo-registered into a single orthophoto. The pre-processing was conducted using the Postflight Terra LT software. The raw images are georeferenced to the Universal Transverse Mercator (UTM), World Geodetic Survey 1984 (WGS-84) coordinate system based on a set of ground control points (GCP) at the field located with a Differential Global Positioning System (DGPS). The GCP are the markers based on the available GPS points and georeference of the image. The plantation is arranged in rows and columns. The numbering of the samples were recorded using the rows and columns and can be rectified from the image. A DTM

data was generated after the georectification and stitching mosaics of the georectified images and then used as input to orthorectified the mosaics of images into a complete full scene orthophoto of RGB and NIR image. The resulted orthophoto images of RGB and NIR were subset to 25 hectares (0.25 km<sup>2</sup>) (the yellow box) is shown in Figure 3.8 (a) and (b) respectively.

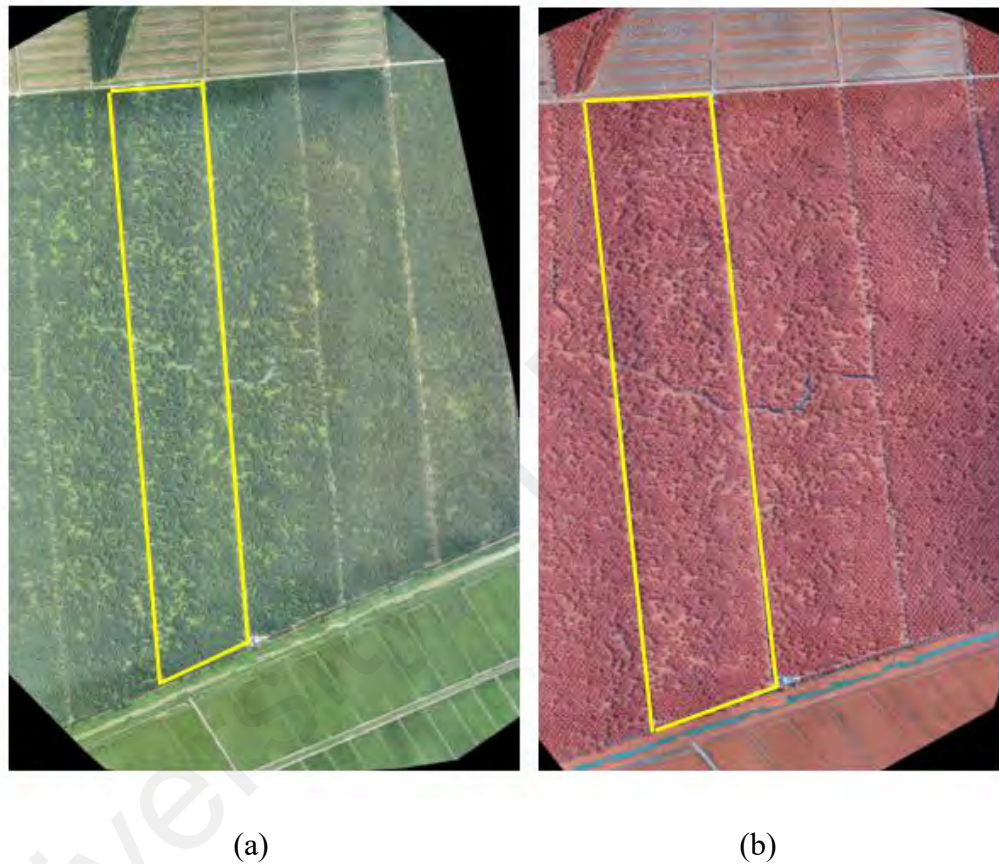


**Figure 3.8: UAV-based multispectral image of oil palm plantation. The yellow box indicates the study area. (a) Digital orthophoto mosaic image of RGB; (b) Digital orthophoto mosaic image of NIR**


### 3.7 Identification of Regions of Interest

Regions of interest (ROIs) are portions of images that are selected graphically as a threshold (ENVI, 2015). The ENVI's procedures allow comparison within the training phase, in order to carry out an unbiased "ground truth" ROIs or images containing areas of labelled data; which were not used accuracy assessment of supervised classification methods (Canty, 2014).

Two main steps to run pixel-based classification are; pre-knowledge (prior knowledge) about the research site and the classification algorithm. The first step was carried out during the field trips for UAV flights and GPS data collection. Seven classes of ground truth materials were used as training data for the supervised classification.

Identification of ROI was extracted containing either oil palm or non-oil palm background from the collected images to evaluate the oil palm classifier. ROI includes training samples (classification image) and test samples (ground truth ROI) for selected classes. The classification accuracy may be affected by some of the errors, including human error, equipment, training samples and sampling procedure. Human errors are the most likely to occur when determining palms *Ganoderma* DSI. This is due to misclassified of the visible symptoms such as fronds wilting, fruiting body and stem rotting. Hence, the field survey should be as close to the time of image acquisition to reduce visual classification errors.

A number of palm crowns were identified and digitised on the multispectral images as the training samples to represent respective classes. Figure 3.9 represents examples of canopy top view for each DSI of the oil palm crown. Based on the figure, it is clearly shown that the severely infected palm (T3) gives the smallest canopy cover compared to the others. The healthy palm (T0) shows the large size canopy followed by the mildly infected palm (T1) and moderate infected palm (T2) that gave a slightly similar size of canopy cover. The size of the canopy decreases in increasing level of DSI (T0 - T3).

<i>Disease Severity Index (DSI)</i>	<i>RGB Image</i>	<i>NIR Image</i>
T0		
T1		
T2		
T3		

**Figure 3.9: Examples of oil palm crown for each oil palm DSI**

In this study, two sets of experiments were used; Experiment 1 and Experiment 2. Experiment 1 consists of T0, T1, T2, T3, vegetation, soil and water bodies. For training samples, 30 samples were used in each class and 10 samples for test samples. The samples were generated in pixels (Table 3.4). T0 has an average area of 49,000 pixels, followed by T1 with 40,000 pixels, T2 with 34,000 pixels and T3 with 25,000 pixels.

**Table 3.5: Numbers of training samples (ROI) and test samples, which were generated in pixels for Experiment 1**

<i>Class</i>	<i>Training</i>	<i>Test</i>
T0	49,260	14,808
T1	40,828	12,849
T2	34,359	11,752
T3	25,318	8,348
Vegetation	12,578	5,310
Soil	6,760	4,837
Waterbodies	5,043	3,707

Meanwhile, for Experiment 2 ROI were classified into healthy, unhealthy, vegetation, soil and water bodies. The healthy class is a combination of T0 and T1 classes, and unhealthy class is the combination of T2 and T3 classes (Table 3.5). The numbers of training samples are the same for both RGB and NIR images. The healthy class has an average area of 90,000 pixels and unhealthy class with 50,000 pixels.

**Table 3.6: Numbers of training samples (ROI) and test samples, which were generated in pixels for Experiment 2**

<i>Class</i>	<i>Training</i>	<i>Test</i>
Healthy	90,021	12,849
Unhealthy	59,629	11,752
Vegetation	12,578	5,310
Soil	6,760	4,837
Water bodies	5,043	3,707

Figure 3.10 shows an example of the ROI Tool in ENVI Classic for the number of training and test samples that were generated in pixels for Experiment 2. Meanwhile, Figure 3.11 shows an example of the distribution of the selected oil palm crown based on the DSI of *Ganoderma* disease in oil palm. Oil palm within the red areas show signs of *Ganoderma* disease infected palm, whereas the green region is healthy palms.

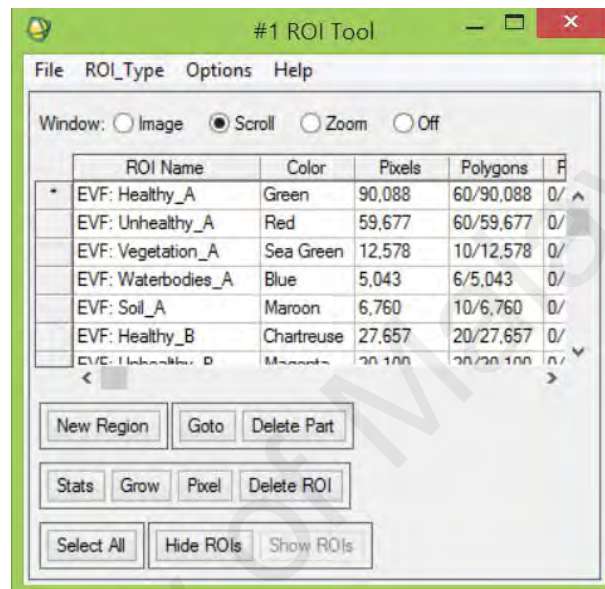


**Figure 3.10: ROI tool that shows the list for training and test samples**

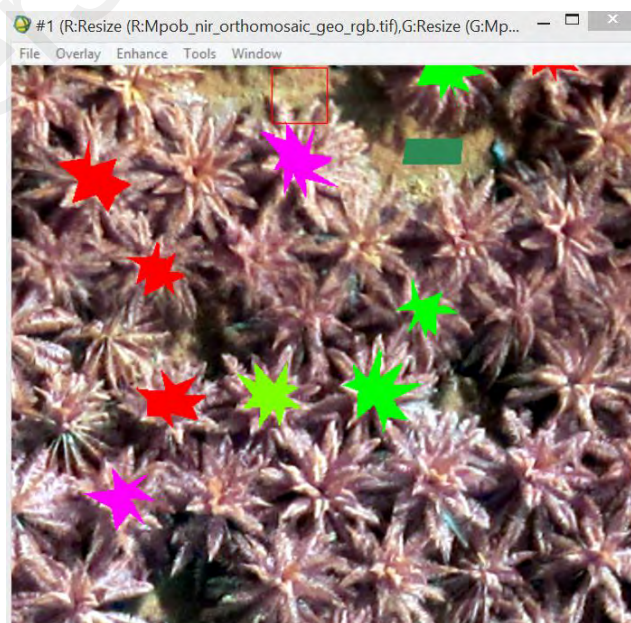


**Figure 3.11: Manual classification of different polygon areas for each class based on the oil palm location**



### 3.8 GIS as Input for Remote Sensing Interpretation

Geographic Information System (GIS) is a computer system for capturing, storing, analysing and displaying geospatial data which describe the locations and characteristics of spatial features (Chang, 2012). A GIS is also a computerised tool for solving geographic problems or an idea that expressed a spatial decision support system (Longley, 2005).

Prior to classification, further processing was done to classify oil palm trees in the image into healthy and unhealthy. The digitisation of *Ganoderma* disease ground data census was done in GIS to overlay and tally digitised census data with orthophoto image. Figure 3.12 shows the overlaying in total of 120 points in shapefile - \*.shp (the file that stores the feature geometry) form which were measured with T0 for healthy palms (30 points), T1 for mild infected palm (30 points), T2 for moderate infected palm (30 points) and T3 for severe infected palm (30 points) in Experiment 1.

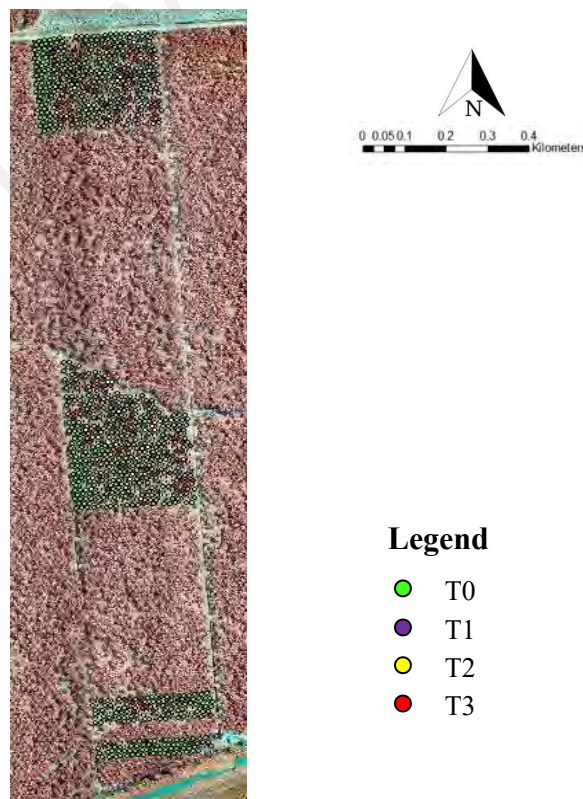


Figure 3.12: Overlaying of 120 points of ground truth in GIS for NIR image

### 3.9 Image Processing

Image classification of remote sensing is the technique of assigning pixels of an image to classes. Generally, it is like assembling identical pixels in a group found in remotely sensed data into classes that match the informational categories by comparing pixels to one another based on user interest (Perumal & Bhaskaran, 2010). The image processing involved several steps which are: 1) applying adaptive filters with different kernel window sizes; 2) supervised classification and 3) accuracy assessment. In this study, several adaptive filters were used to suppress and reduce noise by smoothing while preserving the image sharpness.

#### 3.9.1 Filtering

New pixel values were calculated by using standard deviation based on image pixels within a local box using adaptive filters. In simpler words, the original pixel value is replaced with a new value calculated based on the surrounding valid pixels. The image sharpness detail is still preserved while oppressing noise. Eight different adaptive filters were used in this study and a brief explanation is in Chapter 4. To evaluate the performance of the selected supervised classifications, three types of filter window sizes of  $7 \times 7$ ,  $9 \times 9$  and  $11 \times 11$  were tested on both RGB and NIR images. Speckle degrades the radiometric quality of an image (Mahdavi *et al.*, 2017). It is important to select suitable window size as it should be used to enhance very detail information of an image without having to try several different sizes for an area of interest (Chavez & Bauer, 1982).

These window sizes were selected based on previous study and the accuracy was tested. Previous study stated that the larger the window size, the sharpness and detail of the image is reduced (Argenti, *et al.*, 2013; Purnama *et al.*, 2018).

### 3.10 Supervised Classification

Classification is one of the most important phases of remote sensing image interpretation. Remote sensing supervised classification involves the use of a training dataset consisting of a labelled pixel representative of each category of interest in an image that the classifier needs to be able to recognise and label unseen pixels (Canty, 2014). The labels will represent the classes on the map that requires by the user called thematic map (a map of themes) (Richards, 2017).

To map the *Ganoderma* disease on the multispectral UAV image, three algorithms with different theories were tested namely Maximum Likelihood (ML), Mahalanobis Distance (MD) and Neural Net (NN). Both ML and MD are the usual and conventional classification methods that used simple mathematical principles with different quantifications of distance among samples. Meanwhile, NN is a more comprehensive mathematical mechanism that is widely used in image classification domain. It is an advanced classification algorithm which improves the accuracy of the conventional classification method (Tan *et al.*, 2011; Yuan *et al.*, 2014).

#### 3.10.1 Maximum Likelihood (ML)

Maximum Likelihood (ML) classification is a statistical approach for pattern recognition (Huang *et al.*, 2015). ML assumes that the statistics for each class in each band are normally distributed. The probability is being calculated using a given pixel belongs to a specific class (ENVI, 2015). This classification is the most widely used algorithms when accurate training data are provided in estimating means and variances of the classes and consider the variability of brightness values in each class (Perumal & Bhaskaran, 2010). The ML classification can be calculated by the following discriminant functions for each pixel in the image (Richards, 2012). The ML formula is given by equation (1):

$$g_i(x) = 1n\rho(\omega_i) - \frac{1}{2} \ln |\Sigma_i| - \frac{1}{2} (x - m_i)' \Sigma_i^{-1} (x - m_i) \quad (1)$$

where  $i$  is the  $i$ th class;  $x$  is the  $n$ -dimensional data (where  $n$  is the number of bands),  $\rho(\omega_i)$  is the probability that a class occurs in the image and is assumed the same for all classes,  $|\Sigma_i|$  is the determinant of the covariance matrix of the data in a class,  $\Sigma_i^{-1}$  is the inverse matrix and  $m_i$  is the mean vector of a class.

### 3.10.2 Mahalanobis Distance (MD)

Mahalanobis distance (MD) classification is a faster method over the ML procedure as all of the class covariance are equal (ENVI, 2015). All of the pixels are classified to the closest reference pixels. The MD algorithm assumes that the histograms of the bands have normal distributions (Perumal & Bhaskaran, 2010). It is used to identify and indicate the similarity of an unknown sample set to a known one (Richards, 2012). The MD formula can be written as equation (2):

$$D_i(x) = \sqrt{(x - m_i)' \Sigma_i^{-1} (x - m_i)} \quad (2)$$

where  $D$  is the Mahalanobis distance,  $i$  is the  $i$ th class,  $x$  is the  $n$ -dimensional data (where  $n$  is the number of bands),  $\Sigma_i^{-1}$  is the inverse of the covariance matrix of a class and  $m_i$  is the mean vector of a class.

### 3.10.3 Neural Net (NN)

Lately, much attention has been shifted to the development of more advanced classification algorithm including Neural Net (NN) approach instead of the conventional classification method. NN is a technique that uses the standard back-propagation for supervised learning which consists of one input layer, at least one concealed layer and one output layer (ENVI, 2015). A recursive method was used to back propagate the error through the network and weight adjustment is made (Perumal & Bhaskaran, 2010). In this study, a supervised NN was trained with a back-propagation learning as the best learning method for modelling non-linear relationships.

The NN training is mainly divided into two process which is forward propagation and error back propagation. Firstly, the input feature vector will be calculated in the forward direction, and the output layer is the predicted category obtained. Next, the predicted category is compared with the actual corresponding category to obtain the classification error. Then, the parameters of the NN are trained by the error back-propagation algorithm (Liang *et al.*, 2018).

For the error back-propagation process, the residual  $\delta$  (denotes the contribution to the error) of each layer is calculated first. The formula of the output layer follows the equation (3):

$$\delta_i = a_i(1 - a_i)(a_i - y_i) \quad (3)$$

For the other hidden layers, the formula of  $\delta$  can be written as equation (4):

$$\delta_i^l = a_i^l(1 - a_i^l) \sum_{j=1}^{S_{l+1}} W_{ji}^l \delta_i^{l+1} \quad (4)$$

where  $l$  is the  $l$ th layer of network,  $S_{l+1}$  is number of the neurons of the  $(l+1)$ th layer,  $a_i^l$  is the output value of the  $i$ th unit of the  $l$ th layer.

Figure 3.13 shows an example of parameters of selected classes for ML algorithm. Meanwhile, Figure 3.14 (a) shows the RGB image before applying supervised algorithm, and Figure 3.4 (b) shows the thematic map produced by the ML algorithm.

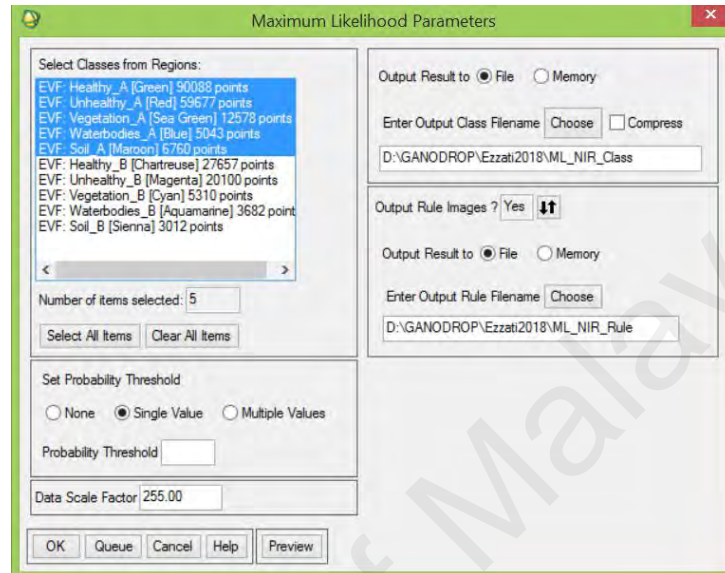
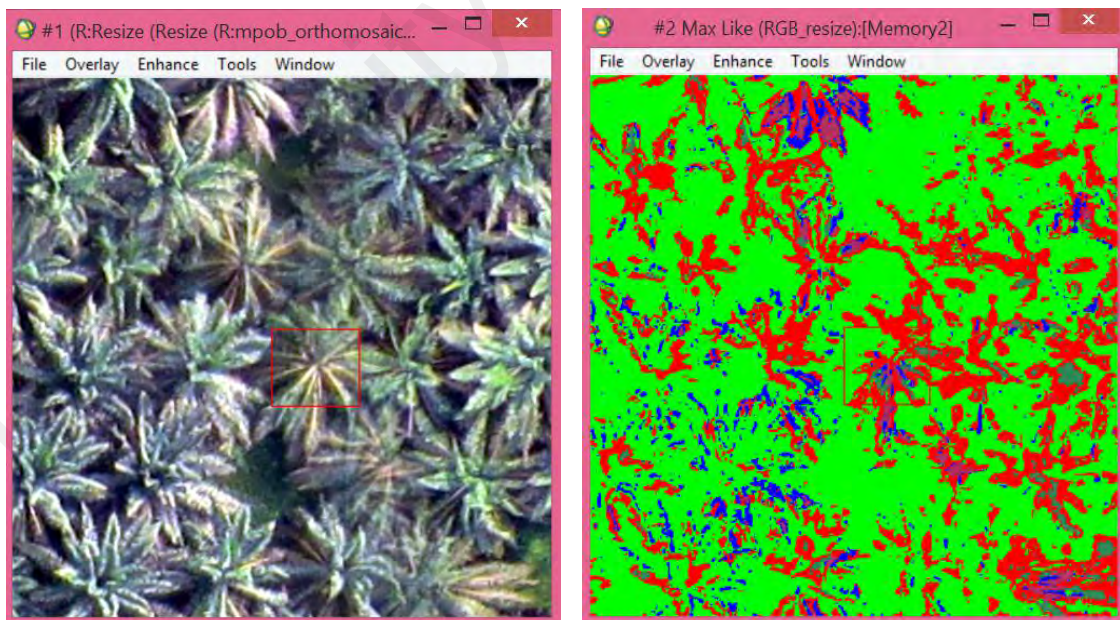


**Figure 3.13: The selected classes for ML parameters**



(a)

(b)

**Figure 3.14: (a) RGB colour image of the oil palm captured by the UAV; (b) Classification thematic map produced by the ML algorithm.**

### **3.11 Accuracy Assessment**

Accuracy assessment measures the map quality that was created from remotely sensed data and is achieved by comparing the classifications made by an algorithm to the known classifications at selected reference locations (Lewis & Brown, 2001; Congalton & Green, 2008). When carrying out analysis, accuracy assessment will help to analyse which classification algorithm is more accurate and more reliable when using reference data collected on the ground, aerial photographs or satellite overpass (Zhang, 2014). Accuracy assessment used confusion matrix derived from validation samples or ROI to test for ML, MD and NN classifiers. Classification accuracy was expressed in terms of the percentage of testing cases correctly allocated by the classifications (Foody & Mathur, 2004).

### **3.12 Confusion Matrix**

Confusion matrix was used to show the accuracy of a classification result by comparing a classification result with ground truth information and accuracy measures based on the correctly classified proportion area that is calculated from the number of pixels that are correctly classified (Lewis & Brown, 2001). In this study, a confusion matrix was calculated using ground truth ROIs. An overall accuracy, producer and user accuracies, and Kappa coefficient are reported in this study.

#### **3.12.1 Overall Accuracy and Kappa Coefficient**

The overall accuracy is calculated by summing up the number of pixels classified correctly and divides by the total number of pixels. The ground truth image defines the true class of the pixels. Accuracy assessment measures the agreement between a standard and a classified map that represents the correctness of the classified map. Overall classification accuracy is given by the following equation (3):

$$\rho = \frac{n}{N} \times 100 \quad (3)$$

where  $p$  is the classification accuracy,  $n$  is the number of points correctly classified on image and  $N$  is the number of points checked in the field.

Meanwhile, the Kappa coefficient is a measure of overall statistical agreement, which takes non-diagonal elements into account. It analyses a single error matrix and compares the differences between various error matrices. The equation (4) for Kappa ( $k$ ) is:

$$k = \frac{pr(a) - pr(e)}{1 - pr(e)} \quad (4)$$

where  $pr(a)$  is the relative observed agreement among raters and  $pr(e)$  is the hypothetical probability of chance agreement, using the observed data to calculate the probabilities of each observer.

The measure of the classification accuracy is through Kappa coefficient statistic. Table 3.6 shows the interpretation of Kappa if the raters are in complete agreement, then  $k = 1$ , and if there is no agreement among the raters,  $k = 0$ .

**Table 3.7: The interpretation of Kappa coefficient (Viera & Garrett, 2005)**

<i>Kappa</i>	<i>Agreement</i>
<0	Less than chance agreement
0.01 - 0.20	Slight agreement
0.21 - 0.40	Fair agreement
0.41 - 0.60	Moderate agreement
0.61 - 0.80	Substantial agreement
0.81 - 0.99	Almost perfect agreement



### 3.12.2 Producer Accuracy and User Accuracy

Producer accuracy and user accuracy can be calculated from the error matrix. An error matrix is an effective way to represent map accuracy which it is a square array of a number set out in rows and columns that express the number of sample units that is assigned to a category in another classification. The reference data (“ground truth”) will represent from the columns, while the classification generated from the remotely sensed data (the map) will be represented from the rows. Moreover, the error matrix can compute other accuracy measures such as overall accuracy, producer’s accuracy and, user’s accuracy.

Overall accuracy is the sum of the correctly classified sample units divided by the total number of sample units in the entire error matrix. Story and Congalton (1986) introduced the producer’s and user’s accuracies to represent the individual category accuracies instead of just the overall classification accuracy.

The overall accuracy between remotely sensed classification and the reference data can be computed as the equation (5):

$$\frac{\sum_{i=1}^k n_{ii}}{n} \quad (5)$$

where,

$$n_{i+} = \sum_{j=1}^k n_{ij}$$

be the samples number classified into category  $i$  in the remotely sensed classification, and

$$n_{+j} = \sum_{i=1}^k n_{ij}$$

be the samples number of classified into category  $j$  in the reference data set.

Producer's accuracy can be computed by equation (6):

$$j = \frac{n_{jj}}{n_{+j}} \quad (6)$$

and the user's accuracy can be computed by equation (7):

$$i = \frac{n_{ii}}{n_{i+}} \quad (7)$$

Figure 3.15 shows an example of the match classes' parameters between training and test samples. Meanwhile, Figure 3.16 shows the class confusion matrix produced with its overall accuracy and Kappa coefficient.

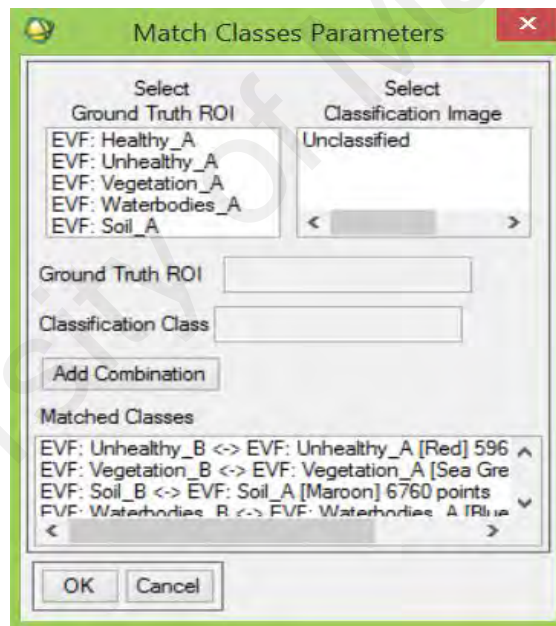


**Figure 3.15: Classes parameters sets for training and test samples**

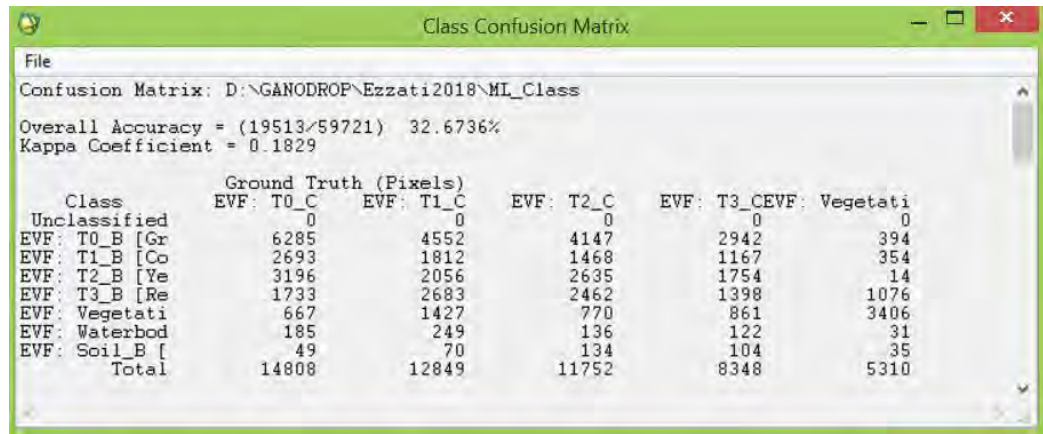


**Figure 3.16: The overall accuracy and Kappa coefficient obtained using confusion matrix**

University of Malaysia

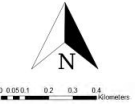
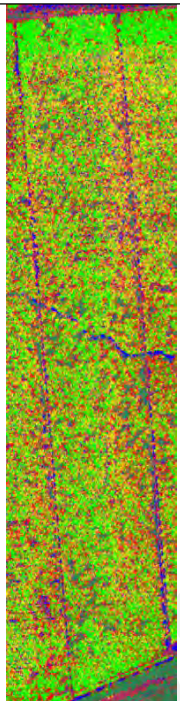
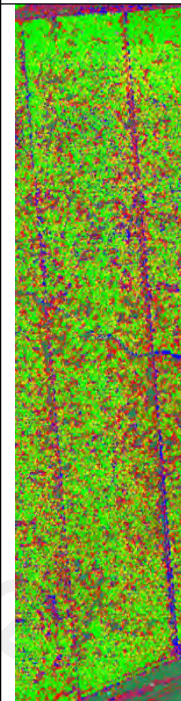
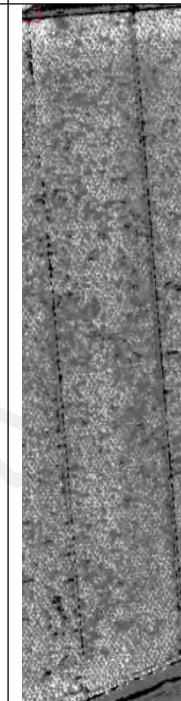
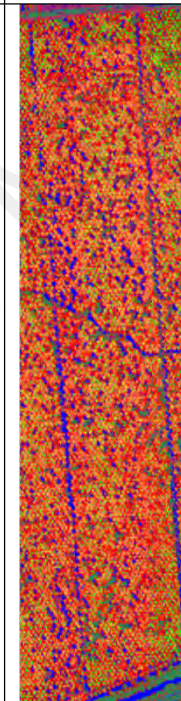
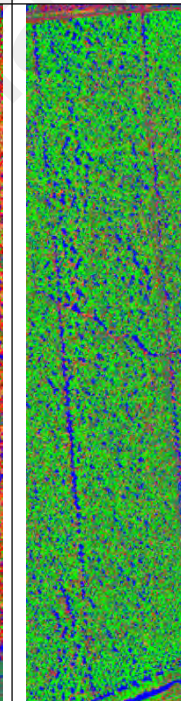
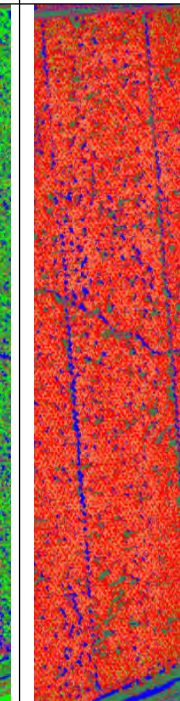
## CHAPTER 4: RESULTS

### 4.1 Adaptive Filters

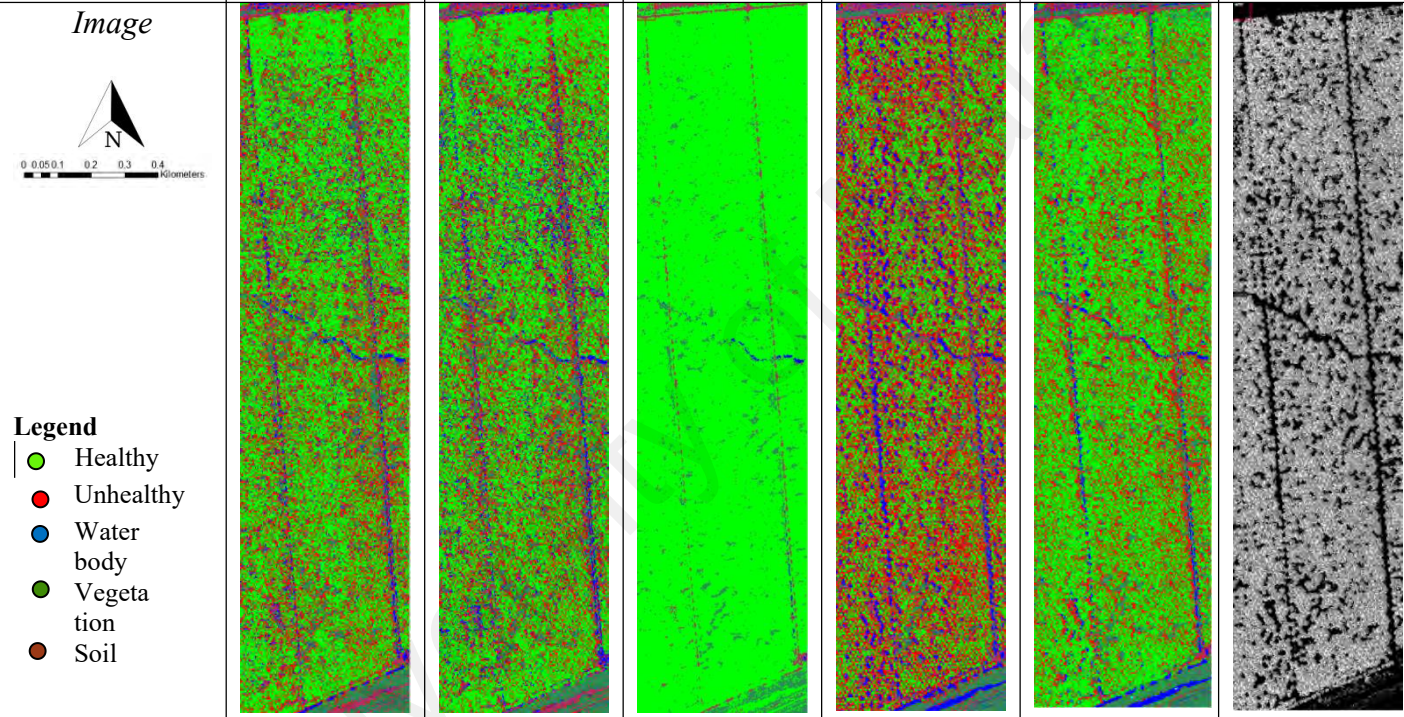
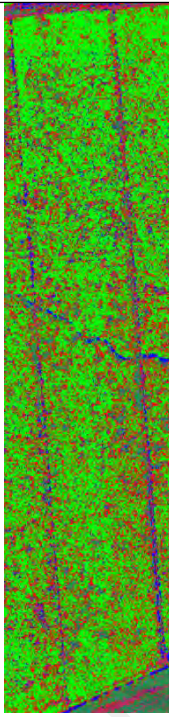
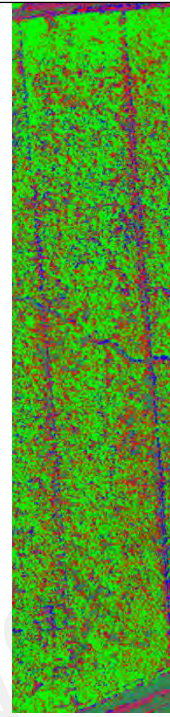
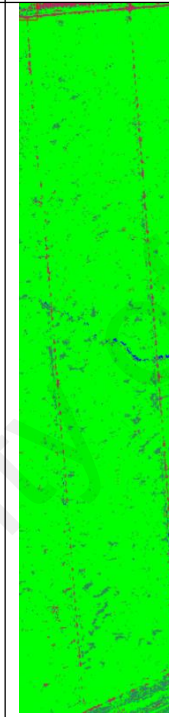
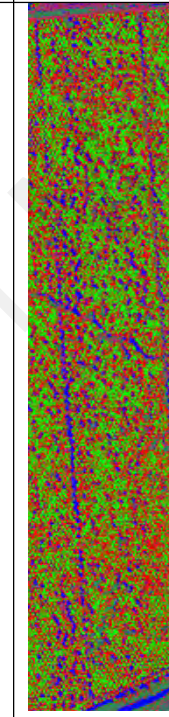
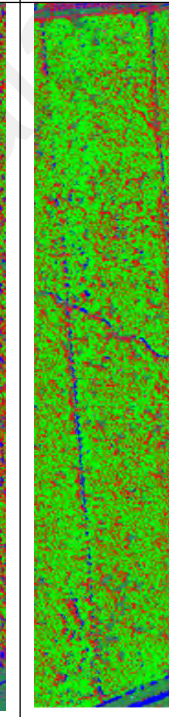
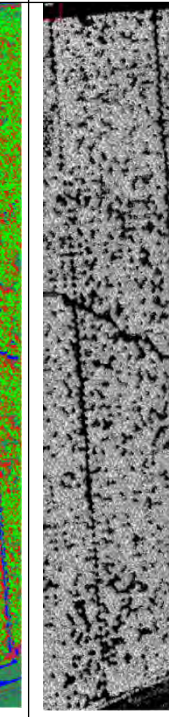
In this study, adaptive filters were used to suppress and reduce noise by smoothing while retaining the image sharpness and important feature. Noise is a natural phenomenon that usually degrades images during the image acquisition and transmission process (Sarode & Deshmukh, 2011). The adaptive filters are considered the most appropriate noise suppression techniques for image processing data. A new pixel value is being calculated from the surrounding valid pixels of the original value (ENVI, 2015). Several adaptation methods are proposed to achieve a better result by the varying window size. A number of adaptive filters were developed to suppress speckle noise in a uniform while preserving the edge information, such as, the Lee filter (Lee, 1980), the Enhanced Lee filter (Lopes *et al.*, 1990), the Frost filter (Frost *et al.*, 1982), the Enhanced Frost filter (Lopes, *et al.*, 1990), the Gamma filter (Kuan *et al.*, 1987), the Kuan filter (Kuan *et al.*, 1985), Local Sigma (Eliason & McEwen, 1990) and Bit Errors (Eliason & McEwen, 1990).

In addition, every adaptive filter used several moving window sizes ( $7 \times 7$ ,  $9 \times 9$  and  $11 \times 11$ ) to study the effect of the window size on the smoothing characteristics and edge preservation.

The filtered images was compared with the original images that are being tested with the classification without any window size. The results of the original image without any filter is shown in Figure 4.1 and 4.2 for RGB and NIR images respectively.

<i>Experiment 1</i>						
<i>Filter</i>	<i>RGB</i>			<i>NIR</i>		
	<i>ML</i>	<i>MD</i>	<i>NN</i>	<i>ML</i>	<i>MD</i>	<i>NN</i>
<i>Image</i>  <b>Legend</b> <ul style="list-style-type: none"> <li><span style="color: green;">●</span> T0</li> <li><span style="color: purple;">●</span> T1</li> <li><span style="color: yellow;">●</span> T2</li> <li><span style="color: red;">●</span> T3</li> <li><span style="color: blue;">●</span> Waterbody</li> <li><span style="color: green;">●</span> Vegetation</li> <li><span style="color: brown;">●</span> Soil</li> </ul>						
<i>Overall Accuracy (%)</i>	32.6736	32.2349	<b>34.4485</b>	<b>40.3491</b>	30.7140	30.5735
<i>Kappa Coefficient</i>	0.1829	0.1771	<b>0.1566</b>	<b>0.2702</b>	0.1690	0.01961

**Figure 4.1: RGB and NIR original images without using filter in Experiment 1**

<i>Experiment 2</i>						
	<i>RGB</i>			<i>NIR</i>		
<i>Filter Image</i>	<i>ML</i>	<i>MD</i>	<i>NN</i>	<i>ML</i>	<i>MD</i>	<i>NN</i>
 <p><b>Legend</b></p> <ul style="list-style-type: none"> <li><span style="color: green;">●</span> Healthy</li> <li><span style="color: red;">●</span> Unhealthy</li> <li><span style="color: blue;">●</span> Water body</li> <li><span style="color: darkgreen;">●</span> Vegetation</li> <li><span style="color: brown;">●</span> Soil</li> </ul>						
<i>Overall Accuracy (%)</i>	51.8528	49.6040	<b>54.7613</b>	<b>58.3407</b>	53.3826	50.4828
<i>Kappa Coefficient</i>	0.2802	0.2510	<b>0.2250</b>	<b>0.3583</b>	0.3104	0.2969

**Figure 4.2: RGB and NIR original images without using filter in Experiment 2**

#### 4.1.1 Lee Filter

The Lee filter was used to smoother noise or speckled data that have an amount of energy transmitted related to the image scene. The Lee filter will suppress noise of the image and still preserves the image sharpness. Besides, the Lee filter will filter data based on statistics calculated within individual filter windows as it is a standard deviation based (sigma) filter (Lee, 1981). The mathematical model for Lee filter is given in equation (8):

$$lmg(i, j) = lm + W * (Cp - lm) \quad (8)$$

where  $lmg$  is the pixel value after filtering,  $lm$  is the mean intensity of filter window and  $Cp$  is the center pixel

#### 4.1.2 Enhanced Lee Filter

The Enhanced Lee was developed by Lopes *et al.* (1990) is a modification of the Lee filter and uses local statistics (coefficient of variation) within individual moving windows. Each pixel is put into one of three classes, including homogeneous, heterogeneous and point target. It reduces the speckle noise effectively by preserving image sharpness and detail. The algorithm follows a formula given by equation (9):

$$L_M * K + P_C * (1-K) \quad (9)$$

where  $P_C$  is the centre pixel value of window,  $L_M$  is the local mean of filter window and  $SD$  is the standard deviation in filter window

### 4.1.3 Frost Filter

The Frost filter differs from the Lee filter as it calculates the new value of the target pixel using a weighted sum of the values within the moving window (Frost *et al.*, 1982). It is a convolutional filter used to remove the multiple noises from images. The weighting coefficients increase as variance within the window increase for the central pixels and decrease with distance from the pixel of interest (Qiu *et al.*, 2004). The Frost filter formula is given by equation (10):

$$DN = \sum_{n \times n} K \alpha e^{-\alpha |t|} \quad (10)$$

where K is the normalized constant,  $|t| = |X - X_0| + |Y - Y_0|$  and n is the moving kernel size

### 4.1.4 Enhanced Frost Filter

The Enhanced Frost filter is a modification from the Frost filter and similarly uses local statistics (coefficient of variation) within individual moving windows in a similar way. The Enhanced Frost filter pixel has the same function as the Enhanced Lee filter for the homogeneous and points target cases (Lopes *et al.*, 1990). The algorithm for Enhanced Frost filter can be defined as equation (11):

$$W(x, y) = e^{-kf_{unc}(C_1(x^1, y^1))|(x, y)|} \quad (11)$$

where  $f_{unc}(C_1(x^1, y^1))$  is a hyperbolic function of  $C_1(x^1, y^1)$



#### 4.1.5 Gamma Filter

The Gamma filter presumes that the pixel original intensity value lies between its intensity value and its actual value of the pixels moving window. The data is gamma distributed instead of a Gaussian distribution. A pixel value is calculated based on local statistics (Shi & Fung 1994). The Gamma filter is similar to Enhanced Frost filter, but if the local coefficient of variation falls between two thresholds, then the pixel value is based on the Gamma estimation of the contrast ratios (Jaybhay & Shastri, 2015).

#### 4.1.6 Kuan Filter

The Kuan filter form is alike as the Lee filter that reduce speckle while preserving image edges, but it is quite advanced than Lee filter in a factor as it has no approximation involved. The filter transforms to an additive noise model from a multiplicative noise model into the additive linear form (Shi & Fung, 1994). Weighted function  $W$  is for Kuan filter is given by the equation in (12):

$$W = \frac{\left(1 - \frac{Cu}{Ci}\right)}{(1 + Cu)} \quad (12)$$

where  $Cu$  is the estimated noise variation coefficient,  $Cu$  is the  $\sqrt{1/ENL}$ , ENL is the equivalent noise looks,  $Ci$  is the variation coefficient of image is the  $Ci$  is the  $S/lm$  and  $S$  is the standard deviation in the filter window

#### 4.1.7 Local Sigma Filter

The Local Sigma filter was used to reduce noise and preserve fine details significantly. The Local Sigma substitutes the pixel being filtered with the mean calculated using the valid pixels within the filter box (Eliason & McEwen, 1990).

#### 4.1.8 Bit Error Filter

The Bit Error filter was used to remove bit-error noise, resulting from noises in the data created by isolating pixels that irrelevant to the image segment. The noise normally gives the image a speckled appearance. To set a valid pixel threshold, mean and standard deviation statistics within the filter box are used (Eliason & McEwen, 1990). The equation for the Bit Error filter is given through formula (13):

$$|P(i,j) - LPF(i,j)| > C\sigma(i,j) \text{ and } |P(i,j) - LPF(i,j)| > TOL \quad (13)$$

where  $P(i,j)$  is a bit error,  $C$  is a constant and the constant  $TOL$  is a minimum threshold value that must be exceeded. Both  $C$  and  $TOL$  are selected as inputs to the program

Figures 4.3 to 4.6 show the results tested on eight adaptive filters using selected three window sizes. The best result of each filter size is highlighted.

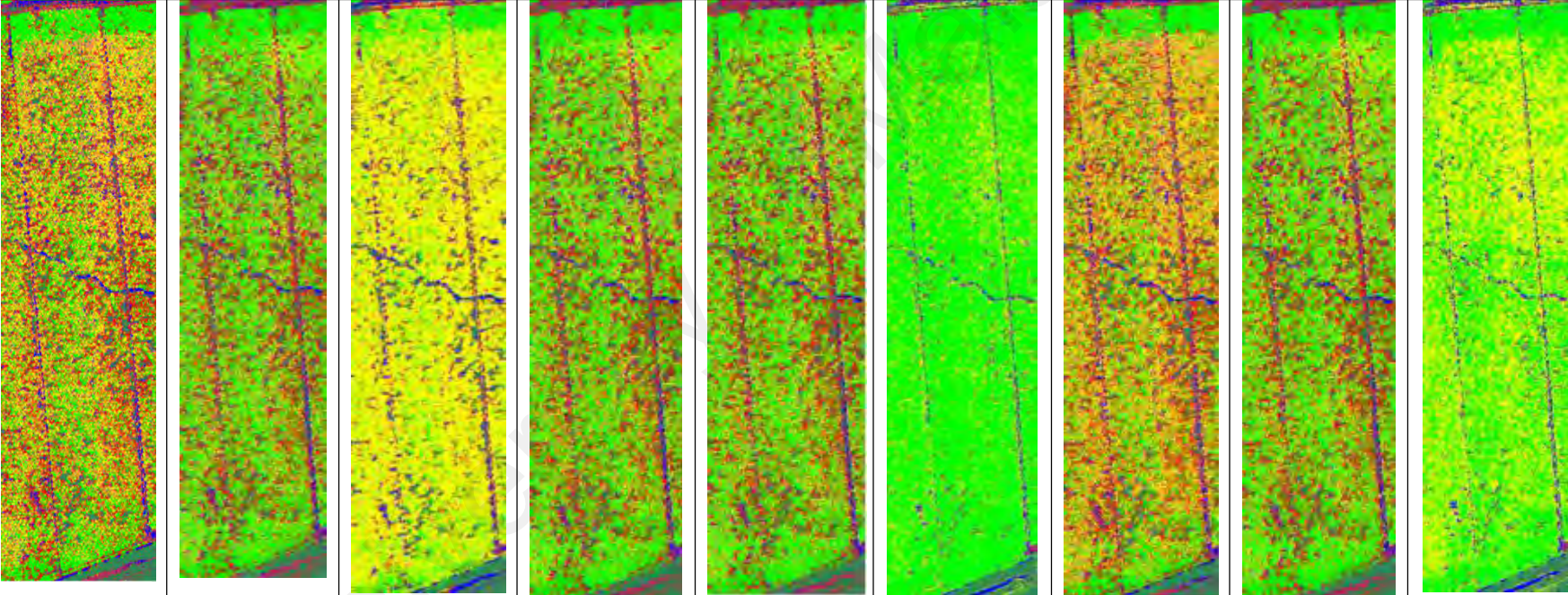
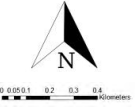
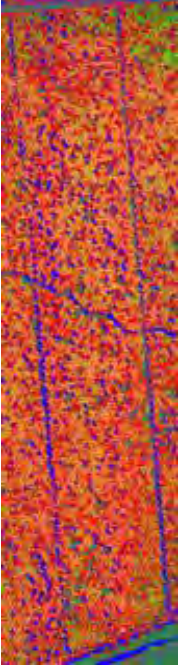
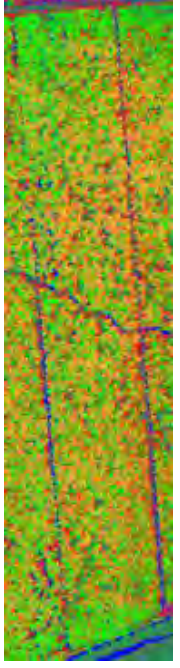
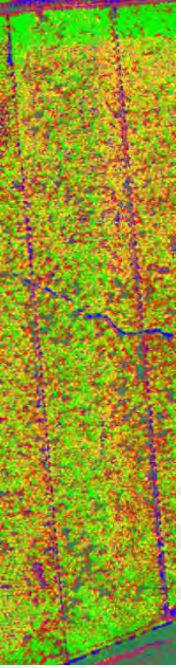
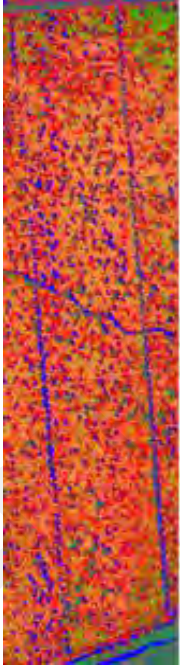
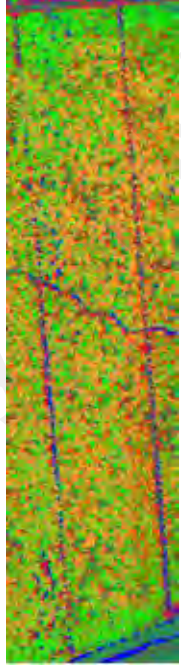
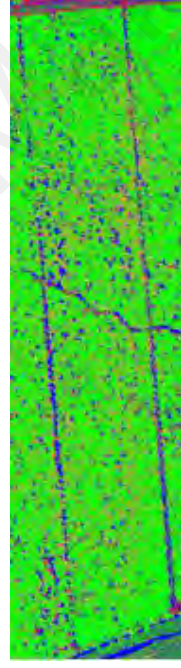
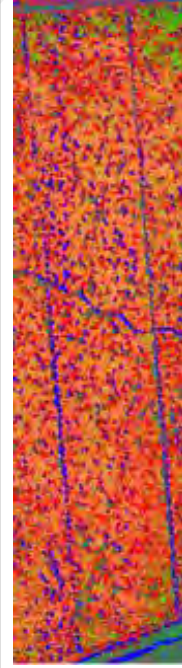
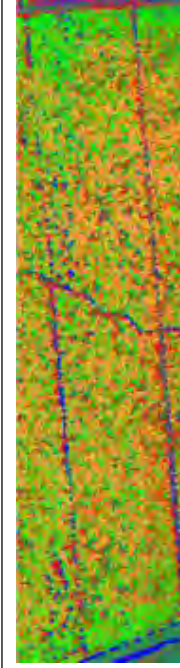
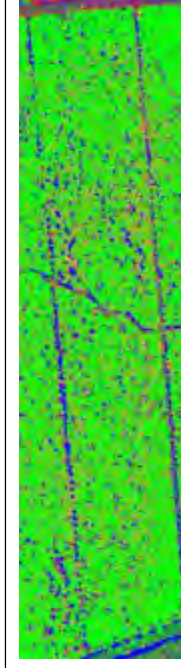
Filter Size	7×7			9×9			11×11		
Filter	Frost	Gamma	Gamma	Enhanced Frost	Enhanced Lee	Enhanced Frost	Enhanced Frost	Frost	Frost
Classifier	ML	MD	NN	ML	MD	NN	ML	MD	NN
<p><i>Image</i></p>  <p><b>Legend</b></p> <ul style="list-style-type: none"> <li>● T0</li> <li>● T1</li> <li>● T2</li> <li>● T3</li> <li>● Water body</li> <li>● Vegetation</li> <li>● Soil</li> </ul>									
<i>Overall Accuracy (%)</i>	33.6732	34.1471	<b>34.4100</b>	34.4502	34.4720	<b>37.5647</b>	34.1974	34.7466	<b>35.9103</b>
<i>Kappa Coefficient</i>	0.1954	0.1981	<b>0.2027</b>	0.2013	0.2016	<b>0.2090</b>	0.2027	0.2048	<b>0.1978</b>

Figure 4.3: Results of RGB image with selected window sizes, filters and classifier in Experiment 1

Filter Size	7×7			9×9			11×11		
Filter	Enhanced Frost	Lee	Lee	Enhanced Lee	Lee	Local Sigma	Gamma	Lee	Local Sigma
Classifier	ML	MD	NN	ML	MD	NN	ML	MD	NN
<p><i>Image</i></p>  <p><b>Legend</b></p> <ul style="list-style-type: none"> <li><span style="color: green;">●</span> T0</li> <li><span style="color: purple;">●</span> T1</li> <li><span style="color: yellow;">●</span> T2</li> <li><span style="color: red;">●</span> T3</li> <li><span style="color: blue;">●</span> Water body</li> <li><span style="color: green;">●</span> Vegetation</li> <li><span style="color: red;">●</span> Soil</li> </ul>									
<i>Overall Accuracy (%)</i>	<b>41.2962</b>	34.8036	41.1941	<b>41.3731</b>	34.7651	40.8561	<b>44.9700</b>	34.7668	40.6821
<i>Kappa Coefficient</i>	<b>0.2824</b>	0.2140	0.2532	<b>0.2836</b>	0.2135	0.2515	<b>0.3369</b>	0.2133	0.2491

**Figure 4.4: Results of NIR image with selected window sizes, filters and classifier in Experiment 1**

Filter Size	7×7			9×9			11×11		
Filter	Enhanced Frost	Frost	Gamma	Frost	Enhanced Lee	Enhanced Frost	Enhanced Frost	Enhanced Frost	Enhanced Lee
Classifier	ML	MD	NN	ML	MD	NN	ML	MD	NN
<p><i>Image</i></p> <p><b>Legend</b></p> <ul style="list-style-type: none"> <li><span style="color: green;">●</span> Healthy</li> <li><span style="color: red;">●</span> Unhealthy</li> <li><span style="color: blue;">●</span> Water body</li> <li><span style="color: darkgreen;">●</span> Vegetation</li> <li><span style="color: brown;">●</span> Soil</li> </ul>									
<i>Overall Accuracy (%)</i>	54.5202	33.6732	<b>57.7318</b>	55.4244	52.5561	<b>57.9444</b>	56.4123	52.9981	<b>58.7499</b>
<i>Kappa Coefficient</i>	0.3158	0.1954	<b>0.2954</b>	0.3298	0.2867	<b>0.2994</b>	0.3449	0.2917	<b>0.3169</b>

Figure 4.5: Results of RGB image with selected window sizes, filters and classifier in Experiment 2

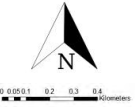
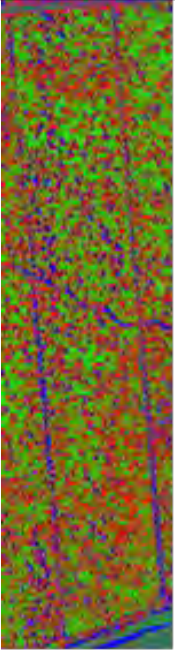
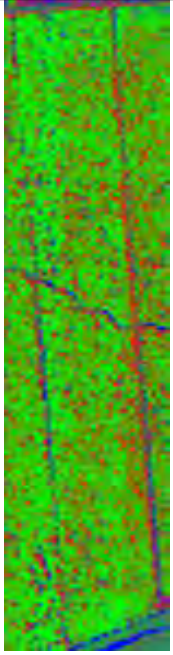
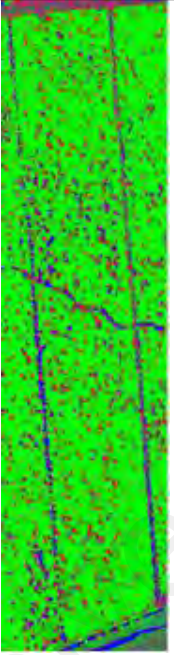
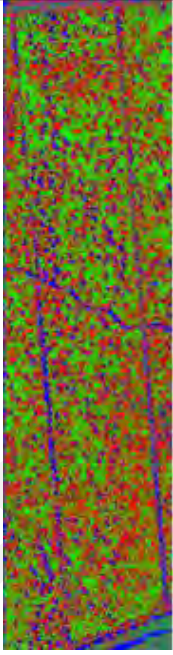
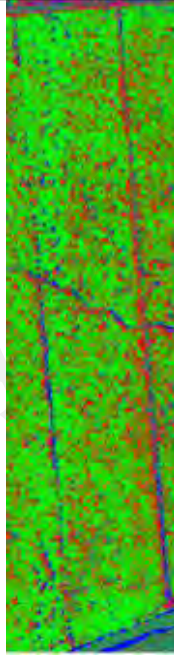
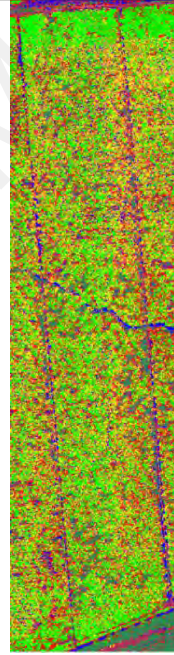
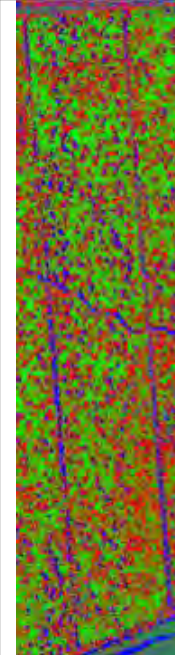
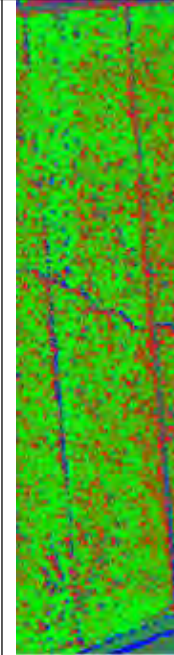
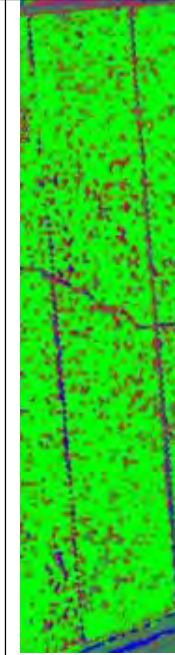
<i>Filter Size</i>	<i>7×7</i>			<i>9×9</i>			<i>11×11</i>		
<i>Filter</i>	<i>Enhanced Frost</i>	<i>Frost</i>	<i>Bit Error</i>	<i>Enhanced Frost</i>	<i>Enhanced Lee</i>	<i>Bit Error</i>	<i>Enhanced Lee</i>	<i>Frost</i>	<i>Frost</i>
<i>Classifier</i>	ML	MD	NN	ML	MD	NN	ML	MD	NN
<i>Image</i>  <b>Legend</b> <ul style="list-style-type: none"> <li><span style="color: green;">●</span> Healthy</li> <li><span style="color: red;">●</span> Unhealthy</li> <li><span style="color: blue;">●</span> Water body</li> <li><span style="color: green;">●</span> Vegetation</li> <li><span style="color: red;">●</span> Soil</li> </ul>									
<i>Overall Accuracy (%)</i>	59.2109	54.5021	<b>62.2496</b>	59.2109	54.5054	<b>62.4136</b>	59.3715	54.3130	<b>62.2446</b>
<i>Kappa Coefficient</i>	0.3727	0.3227	<b>0.3856</b>	0.3750	0.3206	<b>0.3890</b>	0.3757	0.3169	<b>0.3879</b>

Figure 4.6: Results of NIR image with selected window sizes, filters and classifier in Experiment 2

## 4.2 Summary

The overall classification accuracy directly reflects on the chances of the image pixels that are being correctly classified in the classification map. On the contrary, the Kappa coefficient not only considers the correct classification but also the result of omission and commission errors. The performance of the best overall accuracy and Kappa coefficient obtained from the image without filtering along with the eight adaptive filters (Lee, Enhanced Lee, Frost, Enhance Frost, Gamma, Kuan, Local Sigma and Bit Error) with three different window sizes ( $7 \times 7$ ,  $9 \times 9$  and  $11 \times 11$ ) is simplified and highlighted in Table 4.1.

**Table 4.1: The overall accuracy and Kappa coefficient obtained from Experiment 1 and Experiment 2**

<i>Experiment</i>	<i>Image</i>	<i>Filter Size</i>	<i>Classifier</i>	<i>Filter</i>	<i>Overall Accuracy (%)</i>	<i>Kappa Coefficient</i>
<i>Experiment 1</i>	RGB	No filter	NN	N/A	34.45	0.1566
		7×7	ML	Frost	33.67	0.1954
			MD	Gamma	34.15	0.1981
			NN	<b>Gamma</b>	<b>34.41</b>	<b>0.2027</b>
		9×9	ML	Enhanced Frost	34.45	0.2013
			MD	Enhanced Lee	34.47	0.2016
			NN	<b>Enhanced Frost</b>	<b>37.56</b>	<b>0.2090</b>
		11×11	ML	Enhanced Frost	34.20	0.2027
			MD	Frost	34.75	0.2048
	NN		<b>Frost</b>	<b>35.91</b>	<b>0.1978</b>	
	NIR	No filter	ML	N/A	40.35	0.2702
		7×7	ML	<b>Enhanced Frost</b>	<b>41.30</b>	<b>0.2824</b>
			MD	Lee	34.80	0.2140
			NN	Lee	41.19	0.2532
		9×9	ML	<b>Gamma</b>	<b>41.37</b>	<b>0.2836</b>
			MD	Lee	34.77	0.2135
			NN	Local Sigma	40.86	0.2515
		11×11	ML	<b>Gamma</b>	<b>44.97</b>	<b>0.3369</b>
MD			Lee	34.77	0.2133	
NN	Local Sigma		40.68	0.2491		
<i>Experiment 2</i>	RGB	No filter	NN	N/A	54.76	0.2250
		7×7	ML	Enhanced Frost	54.52	0.3158
			MD	Enhanced Frost	52.09	0.2813
			NN	<b>Gamma</b>	<b>57.73</b>	<b>0.2954</b>
		9×9	ML	Frost	55.42	0.3298
			MD	Enhanced Lee	52.56	0.2867
			NN	<b>Enhanced Frost</b>	<b>57.94</b>	<b>0.2994</b>
		11×11	ML	Enhanced Frost	56.41	0.3449
			MD	Enhanced Frost	53.00	0.2917
	NN		<b>Enhanced Lee</b>	<b>58.75</b>	<b>0.3169</b>	
	NIR	No filter	ML	N/A	58.34	0.3583
		7×7	ML	Enhanced Frost	59.21	0.3727
			MD	Frost	54.50	0.3227
			NN	<b>Bit Error</b>	<b>62.25</b>	<b>0.3856</b>
		9×9	ML	Enhanced Frost	59.21	0.3750
			MD	Enhanced Lee	54.51	0.3206
			NN	<b>Bit Error</b>	<b>62.41</b>	<b>0.3890</b>
		11×11	ML	Enhanced Lee	59.37	0.3757
MD			Frost	54.31	0.3169	
NN	<b>Frost</b>		<b>62.24</b>	<b>0.3879</b>		



## CHAPTER 5: DISCUSSION

### 5.1 Introduction

In this section, the results of supervised classifications using UAV-based images of the red-green-blue (RGB) and the near-infrared (NIR) towards *Ganoderma* disease severity index (DSI) were discussed. The discussion includes (1) multispectral bands versus hyperspectral bands, (2) training samples classification, (3) window size of the adaptive filter, (4) supervised classification, and (5) classification results.

The results of each classifier were presented in Chapter 4. The results tabulated in Table 4.1 shows that the Bit Error filter had the highest accuracy in giving better classification accuracy, followed by Enhanced Lee, Gamma, Enhanced Frost, Frost, Lee and Local Sigma. Meanwhile, Kuan filter was considered unsatisfactory for the analysis. In Experiment 1, for most of the classification, Gamma is the best filter. Meanwhile, Bit Error gives higher accuracy compared to other filters in Experiment 2, followed by Frost and Enhanced Lee when the image was classified using the NN classifier.

The range of accuracy of the analysis for RGB orthophoto image in Experiment 1 is considered low, from 33.67% to 37.56% only. Meanwhile, analysis of NIR orthophoto image in Experiment 1 provides better classification accuracy compared to RGB orthophoto ranging from 34.77% to 44.97%, but still categorised as low overall accuracy for mapping *Ganoderma* disease detection in oil palm.

Moreover, this study proposes the improvement of the performance of the classification techniques by applying adaptive filters. The advantage of using window size is that such filters adequate performance at reducing noise and preserving edges. Results show that the performance obtained with adaptive filters are better than the classification results of the images that is not applied with filter.

In Experiment 2, the RGB orthophoto image classification showed that there are similar ranges of the accuracy from the three filter sizes  $7 \times 7$ ,  $9 \times 9$  and  $11 \times 11$ . A well-performing filter presents high overall accuracy and Kappa coefficient. The  $7 \times 7$  filter size of Gamma is the most appropriate filter and provided accuracy from 52.09% to 57.73%. Meanwhile, analysis using  $9 \times 9$  filter size for RGB orthophoto image showed that the most suitable filters are Enhanced Frost, Frost and Enhanced Lee which gives an accuracy ranging from 52.56% to 57.94%. For  $11 \times 11$  filter size, Enhanced Lee gives the best result and the accuracy ranging from 53.00% to 58.75%.

Further analysis of the NIR orthophoto image in Experiment 2 showed different results. The results showed better accuracy compared to the RGB orthophoto image classification. The accuracy was moderate, ranging from 54.31% to 62.41%. The best accuracy of 62.41% was obtained from NIR orthophoto image filtered using Bit Error with  $9 \times 9$  filter size. Both of the multispectral images can be used to determine the range of the vegetation properties that involve the colour changes which associated with a diseased plant that can be easily detected in the NIR wavelength before it can be observed in the visible spectrum (Heaphy *et al.*, 2017).

However, the accuracy does not achieve a good classification accuracy standard of more than 80% as suggested by many researchers. The results also agreed with Minarik & Langhammer (2016) that studied the detection and tracking of forest disturbance dynamics using multispectral UAV photogrammetry. Their results suggested that RGB and NIR images from UAV also had a moderate result to discriminate and identify forest disturbance dynamics. Other than that, a study conducted by Lehmann *et al.* (2015) on coloured infrared images over the forest area to monitor pest infestation levels also showed a moderate accuracy of classification with 0.66 and 0.67 of Kappa coefficient. They suggested that the low to moderate accuracy may due to a high diversity of forest branch texture and an inadequate number of spectral bands.

Zhang *et al.* (2005) also suggested the same conclusion where multispectral or multiband images cannot distinguish between all disease severities of late blight disease in tomato fields. Their results suggested that the multispectral images can only successfully detect the third level of late blight disease in tomato. Other than that, Garcia-Ruiz *et al.* (2013) used six spectral bands camera mounted on UAV to detect Huanglongbing in orange trees. Their results also suggested moderate results (28-45% and 61-74%) for certain study areas.

## 5.2 Multispectral Bands versus Hyperspectral Bands

Based on the results in Chapter 4, the low and moderate accuracies for both experiments was mainly due to the low number of spectral bands. There is a common doubt as to whether wide band multispectral data can detect *Ganoderma* disease that might be always obvious in narrow hyperspectral band. In this study, it was proved that the *Ganoderma* disease can be detected with moderate accuracy from the DSI classification of *Ganoderma* disease severity index using RGB and NIR orthophoto images. The main cause that influences the accuracy is the small number of spectral bands that have a wide bandwidth that reduces the detectability and ambiguities between the DSIs. The higher numbers of spectral bands are able to improve image classifiers to perform better classification because the continuous spectral in the bands retains a lot of spectral information of the target.

Previous research conducted by Nisfariza (2012) were able to detect the *Ganoderma* disease up to non-visible symptoms using hyperspectral remote sensing. The *Ganoderma* can be detected by a number of the wavelengths specific to the disease using hyperspectral data. The study was able to distinguish a number of wavelengths specific to the disease detection for early detection of *Ganoderma* disease in oil palm using statistical tests of the significance between pairs of disease classes; T1 (uninfected

palm), T2 (infected palm with *Ganoderma spp.* without foliar symptoms) and T3 (infected palm with *Ganoderma spp.* with foliar symptoms). The result demonstrates great potential to detect *Ganoderma* disease over large infected oil palm area using the hyperspectral sensor.

### 5.3 Training Samples Classification

Experiment 2 was classified into two classes of DSI, thus it shows higher results compared to Experiment 1 that were classified into four classes of DSI. Generally, the overall accuracy increased as the number of classes decreased. The results in Experiment 2 shows poor spectral separability between subclasses and produced higher Kappa values. The combined classes of T1, T2 and T3 into one class improved the classification results.

In this study, the landscape of the study area is complex since the distributions of the *Ganoderma* DSI are heterogeneous. Thus, selecting sufficient training samples become difficult. Since the data used in this study are of high spatial resolution images for classification, mixed pixels are less occurring. Hence, the selection of training samples must take into consideration the availability of ground reference data, the study area landscapes and the spatial resolution of the image being used.

#### 5.4 Window Size of the Adaptive Filter

Among the eight adaptive filters, the best filter in this study is the Bit Error filter that has a good performance in reducing noise and proves its good abilities in speckle suppression and detail preservation. This is because the Bit Error filter remove random bit errors which is the pixel values with no relation to the image scene and it smooth noisy data that are pixels related to the image scene (Eliason & McEwen, 1990).

To maintain the quality of the image while reducing the multiplicative noise, the used of the adaptive filters include an adaptive window filter that is adjusted in each position of the image. Filter window sizes of  $9 \times 9$  and  $11 \times 11$  show a good result compared to  $7 \times 7$ . Even though the  $11 \times 11$  window size also shows a higher value,  $9 \times 9$  is selected because it has a less smoothing effect. From the analysis, the range of window sizes which are selected for filtering shows that the minimum window size is more significant than the maximum window size. Besides, results do not increase when window size increase. Even though the performance of the adaptive filter is not the best, it has a higher performance above 60% that is obtained with a  $9 \times 9$  window size.

A window size of  $13 \times 13$  was also tested on NIR image using the best filter result from Experiment 2, which is the Bit Error and applied using the NN algorithm. The overall accuracy obtained and Kappa coefficient is 50.71% and 0.2879 respectively. Meanwhile, the RGB image being tested with Enhanced Lee filter which is the best filter obtained in Experiment 2 for RGB image with  $13 \times 13$  window size. The overall accuracy result is 57.42% with 0.2816 of Kappa coefficient. It is evident that the window size gives effect to the filter's performance. This is due to the added window size is too large, it would affect to reducing sharpness and detail of an image (Mahdavi *et al.*, 2017). Hence, it is important to select the minimal window size, and the most suitable choice in this study is  $9 \times 9$ .

## 5.5 Supervised Classification

Based on the overall accuracy and Kappa coefficient of the three classification methods performance, NN classification method can be concluded to be the most accurate regardless of RGB and NIR images. This indicates that NN classifier is capable to classify *Ganoderma* DSI of oil palm using UAV image mosaic, followed with ML classifier. Meanwhile, the MD classifier is found to be the least accurate.

The NN classifier performed better than the ML classifier based on the visual interpretation of a classified map, as well as the percentage of the classification accuracy. This shows that the experience of the NN classifier tends to become more accurate than the statistical ML technique. Previously, Joshi *et al.* (2006) reported that the NN classifier can increase the classification accuracy compared to ML technique by 15% in their forest canopy density study. In this study, the classification accuracy could be increased up to 5-13% when using the NN classifier. The increasing of the classification accuracy is due to the ability of NN in handling the mixed pixel problem in the image. Moreover, the image used in this study were obtained from high spatial resolution and much information could be extracted from the image (Mustapha *et al.*, 2010).

In terms of processing time, the NN was slower than ML and MD in the training phase. However, once the training phase is completed, the classification of the images become faster. These three classifiers considered fast in the training and classification phases. NN does not require much training set for the classification process as the classifier is not a statistical approach, unlike ML and MD that needs many training data for the classification process. Thus, statistical distribution from large training sets can be generated for classifying the images.

A different form of classifiers such as parametric classifiers (ML and MD) and non-parametric classifier (NN) have their own advantages and limitations. An ML classifier may provide an accurate classification result when sufficient training samples are available in a dataset. Apart from that, when an image data is anomalously distributed, NN classifier demonstrates a better classification result (Lu & Weng, 2007).

## 5.6 Classification Results

The results illustrate that the NIR image mosaic produced better supervised classification results compared to RGB image mosaic. The additional NIR band improves the image classification performance because chlorophyll pigment absorbs more energy in the red region. NIR reflectance is high because palm canopies strongly scatter the NIR energy, whereas RGB reflectance is typically low because of the absorption properties of pigments (Ollinger, 2011).

Healthy palms appear green since the green light band is reflected effectively compared to red, blue and yellow bands, which absorbed by protective pigments. Diseased palms usually exhibit discrete lesions on leaves corresponding to necrotic regions, which increases reflectance in the visible range (West *et al.*, 2003).

The uses of UAV promote remote sensing technology in monitoring and detection of palms infected with *Ganoderma boninense* that existed in oil palm plantation plot. The foliar symptoms of *Ganoderma* are prominent and visible at certain levels of infection and can be discerned through the human eyes. The basic visual concept is applied to RGB image since it corresponds to a human eye optical concept. Meanwhile, the use of NIR filter in the UAV is additional whereby it implies the high reflectance of vegetation in the NIR region that is invisible to the human eye to demonstrate the health of the palms.

## 5.7 Conclusion

Even though the UAV Swinglet provides a fine spatial resolution, the limitation of UAV multispectral is the difficulty in distinguishing between certain vegetation classes. Diagnostic analysis towards *Ganoderma* disease has been a challenging issue with multispectral remote sensing sensor as it can only detect plant symptoms such as the effect of the disease on leaf and canopy rather than the cause of the symptoms.

University of Malaya



## CHAPTER 6: CONCLUSION

### 6.1 Introduction

In this study, the supervised classification techniques have been used to map the distribution of *Ganoderma* disease in oil palm plantation using high resolution digital images acquired from the Swinglet platform. This study also sought to see whether small, inexpensive Unmanned Aerial Vehicle (UAV) with high quality data can be used to mosaic and perform in the supervised classification of small areas.

The performance of various classifiers was compared and based on the high overall accuracy and moderate Kappa coefficient, Neural Net (NN) classifier outperformed Maximum Likelihood (ML) and Minimum Distance (MD) classifiers to produce classified oil palm healthy and disease infected thematic map. Thus, NN classification method was superior in performance due to the ability of NN in handling the mixed pixel problem in the image (Tan *et al.*, 2011). The poor performance of the MD classifier may be due to the classes of DSI being segregated are very similar (healthy, mild infection, moderate infection and severe infection). Besides, the ML and MD classifiers are non-parametric and are less sensitive to the distributions of the input data.

Both of the experiments showed that the NIR image gives better performance compared to RGB image. Separating fronds wilting in an RGB image is a difficult task even for a human observer. Hence, the additional NIR wavelength can associated with a diseased plant long before the changes are observed in the visible spectrum.

Besides that, the higher the window size used in the classification was determined as a better result, instead of a smaller window size. However, the window size of 9×9 much preferred compared to 7×7 and 11×11 filter sizes. This is due to a small window size exaggerates the difference between the moving windows, increasing the noise

content on the texture image. Meanwhile, too large window size cannot extract texture information effectively due to smoothing the texture variation. Besides, more processing time implies a large window size (Lu & Batistella, 2005).

The results show that some of the adaptive filters are able to preserve the mean of an oil palm area to a satisfactory level. However, when looking at the speckle suppression, the filtering algorithm of the Bit Error using window size of  $9 \times 9$  outperformed the other adaptive filters. Meanwhile, Local Sigma and Kuan filters appear not to be able to significantly reduce speckle noise. The Bit Error filter performed best for extracting the *Ganoderma* disease using NN classifier. The filter that is most suitable depends on the requirements of the application.

Experiment 2 showed the best result towards evaluating *Ganoderma* disease in RGB and NIR images in contrast to Experiment 1, as the lower number of categories provide better classification accuracy compared to many disease categories due to less number of spectral bands. It is necessary to make a reclassification process, which mixing more than one cluster in one class to obtain a predefined number of classes that are resulting in more sensitive detection (Poblete-Echeverría *et al.*, 2017). The results show the potential of the lower number of categories for mapping the *Ganoderma* disease, but also reveal the limitations of this classification system, especially in relation to the level of accuracy for mapping between healthy and disease palms from other land cover types with similar spectral signatures.

## 6.2 Recommendations

This study fills the gap in the literature by developing a systematic method of UAV techniques for mapping the *Ganoderma* disease in oil palm plantation. This study also explores the potential of the high accuracy UAV remote sensing techniques.

Overall, the UAV presented in this study shows the capability for mapping the *Ganoderma* disease in oil palm plantation as UAV offers excellent potential at low cost in terms of spatial data. Nevertheless, there is also a limitation in this study that it has been demonstrated that multispectral images gathered by UAV can be used, but only with a moderate outcome. This is due to the limitation in terms of the classification methods used, and other supervised classification algorithms might be more accurate but have not been tested in this study.

Few recommendations can be used to improve the accuracy of the results. Firstly, by reconsider of using other non-linear and non-parametric supervised advanced machine learning classifiers such as support vector machine (SVM) and random forest (RF) algorithms. SVM algorithm is a pattern recognition method and mainly used for classification and regression of non-linear and high-dimensional samples. Meanwhile, the RF algorithm is a classification tree algorithm and can handle high-dimensional data which affects the sample classification and limit interactions between features (Yuan *et al.*, 2017). Moreover, object-based image analysis (OBIA) can also be reconsidered since it is thought to be more effective than the pixel-based method when handling high resolution image. From these methods, the precision, accuracy, and stability between models can be compared to give the best result.

Secondly, the statistical significance of differences between the overall accuracy of the non-parametric techniques can be assessed using the McNemar's test, which considers the testing sample set is common to all classifiers (Mallinis *et al.*, 2014).

Lastly, it is recommended to acquire additional bands for multispectral image since the data used in this study have the limitation of a number of bands. By increasing the number of bands to an estimation model, the results will in turn see an increment.

### **6.3 Future Work**

This study has shown a prospect of *Ganoderma* disease research using UAV with RGB and NIR images as UAV are getting increasingly popular in agriculture as they represent a cost-effective and support decision-making. However, the multispectral sensor only provides information on a very limited number of bands which might not sufficient in an area.

This study opens a new possibility for new research on UAV carrying the hyperspectral sensor that can generate hundreds of bands in a spatial resolution image to obtain important information that can enhance the accuracy of a model. However, the usage of hyperspectral UAV is still scarce compared to other sensors involving UAV as the high prices of high-resolution spectroscopy that can compromise cost-effectiveness (Adão *et al.*, 2018). Multispectral remote sensing can only detect when the effects of the disease are prominent, contrary to the hyperspectral image that offers great potential at determining the changes in symptoms at an early stage (Qi *et al.*, 2016).

Besides, future work can also venture in radio detection and ranging (RADAR) imaging using a UAV platform for *Ganoderma* disease detection research in oil palm. Selected bands from previous studies from Nisfariza (2012) can be used for *Ganoderma* disease detection.

#### 6.4 Conclusion

UAV makes an ideal platform to gather data required for agricultural practices. The vast expanse of remote sensing technology for early detection tools are more sensitive and precise with standardising methods. By using UAV, we may know at what level the *Ganoderma* disease has spread that is prior to human eye since farmers and experts usually observe, detect and identify the infected plants with the naked eye that is time consuming and inaccurate.

In conclusion, the UAV-based image has bridged the gap between ground-based observations and remotely sensed image from conventional aircraft and satellite platforms in the use for *Ganoderma* disease detection in oil palm plantation where fieldwork is tedious. With the advancement of UAV technology, this technology will bring benefit to settlers for the early control management for *Ganoderma* disease since UAV can perform the ground census aerial that provides fast and accurate results. It is important to have a classification technique based on aerial imaging that can detect and locate oil palm *Ganoderma* disease in near real-time. The usage of UAV have the capability to be developed into a powerful tool for the Malaysian government to monitor the *Ganoderma* disease of oil palm plantation nationwide for fast actions.

## REFERENCES

- Abu Sari, N., Abu Sari, M. Y., Ahmad, A., Sahib, S. & Othman, F. Using LAPER quadcopter imagery for precision oil palm geospatial intelligence (OP GeoInt). *Journal of Telecommunication, Electronic and Computer Engineering*, 10(1), 25-33.
- Adão, T., Hruska, J., Padua, L., Bessa, J., Peres, E., Morais, R. & Sousa, J. J. (2017). Hyperspectral imaging: a review on uav-based sensors, data processing and applications for agriculture and forestry. *Remote Sensing*, 9(11), 1110.
- Aik, C. S. (2015). Breeding and genetics of the oil palm. In Lai, O. M., Tan, C. P. & Akoh, C. C. *Palm oil: production, processing, characterization, and uses*. Elsevier.
- Argenti, F., Lapini, A., Bianchi, T. & Alparone, L. (2013). A tutorial on speckle reduction in synthetic aperture radar images. *IEEE Journals & Magazines*, 1, 6-35.
- Arif, M. S., Roslan, A. & Idris, A. S. (2011). Economics of oil palm pests and *Ganoderma* disease and yield losses. In: *Proceedings of the Third MPOB-IOPRI International Seminar: Integrated Oil Palm Pests and Diseases Management*.
- Ariffn, D., Idris, A.S. & Khairuddin, H. (1993). Confirmation of *Ganoderma* infected palm by drilling technique. *Proceeding of the 1993 PORIM International Palm Oil Congress: Update and Vision (Agriculture)*. pp. 735-738.
- Astina, T., Wahid, A. R., Akmal, M. S., Othman, Z., Razak, A. M. Y., Zulkarnain, M. A. R., Nasruddin, A. S. & Norhadija, D. (2015). Oil palm tree growth monitoring for smallholders by using unmanned aerial vehicle. *Journal of Technology (Sciences & Engineering)*, 77(26), 17-27.
- Barcelos, E., Rios, S. A., Cunha, R. N. V., Lopes, R., Motoike, S. Y., Babiychuk, E., Skiryecz, A. & Kushnir, S. (2015). Oil palm natural diversity and the potential for yield improvement. *Frontiers in Plant Science*, 190(6). doi: 10.3389/fpls.2015.00190
- Basri, M. W., Norman, K., Idris, A. S., Ariffn, D., Shamala, S., Ramle, M. & Siti Ramlah, A. A. (2003). *Handbook of pests and diseases of oil palm*. Selangor, Malaysia: Malaysian Palm Oil Board.

- Bulanon, D. M., Horton, M., Salvador, P & Fallahi, E. (2014). Apple orchard monitoring using aerial multispectral imaging. *American Society of Agricultural and Biological Engineers*, 1-10. doi: 10.13031/aim/20141913165
- Calderón, R., Navas-Cortés, J. A., Lucena, C. & Zarco-Tejada, P. J. (2012). High-resolution airborne hyperspectral and thermal imagery for early detection of Verticillium wilt of olive using fluorescence, temperature and narrow-band spectral indices. *Remote Sensing of Environment*, 139, 231-245.
- Campbell, J. B. & Wynne, R. H. (2011). *Introduction to remote sensing*. Guilford Press.
- Candiago, S., Remondino, F., De Giglio, M., Dubbini, M. & Gattelli, M. (2015). Evaluating multispectral images and vegetation indices for precision farming applications from UAV images. *Remote Sensing*, 7, 4026-4047.
- Canty, M. J. (2014). *Image analysis, classification and change detection in remote sensing: with algorithms for ENVI/IDL and Python, Third Edition*. CRC Press.
- Chang, K. T. (2012). *Introduction to geographic information systems*. Singapore: McGraw-Hill.
- Chavez, P. & Bauer, B. (1982). An automatic optimum kernel-size selection technique for edge enhancement. *Remote Sensing of Environment*, 12, 23-38.
- Chaves, A. A., La Scalea, R. A., Colturato, A. B., Kawabata, C. L. O., Furtado, E. L. & Castelo Branco, K. R. L. J. (2015). Using UAVs and digital image processing to quantify areas of soil and vegetation. In *4th International Conference of Mathematical Modeling in Physical Sciences (IC-MSquare2015)*. IOP Publishing Ltd. doi: 10.1088/1742-6596/633/1/012112
- Chong, K. P., Dayou, J. & Alexander, A. (2017). Pathogenic nature of *Ganoderma boninense* and basal stem rot disease. In: *Detection and control of Ganoderma boninense in oil palm crop*. Springer Briefs in Agriculture. Springer, Cham. doi: 10.1007/978-3-319-54969-9
- Chuvieco, E. & Huete, A. (2010). *Fundamentals of Satellite Remote Sensing*. Britain: Blackwell Science Ltd.
- Congalton, R. G. & Green, K. (2008). *Assessing the accuracy of remotely sensed data: principles and practices*. CRC Press.

- Corley, R. H. V. & Tinker, P. B. H. (2003). *The oil palm*. Blackwell Science Ltd.
- Corley, R. H. V. & Tinker, P. B. H. (2008). *The oil palm*. John Wiley & Sons.
- Corley, R. H. V. & Tinker, P. B. H. (2015). *The oil palm*. John Wiley & Sons.
- Curran, P. J. (1985). *Principles of remote sensing*. Longman Inc.
- Duzgun, H. S. & Demirel, N. (2011). *Remote sensing of the mine environment*. CRC Press.
- Eliason, E. M. & McEwen, A. S. (1990). Adaptive box filters for removal of random noise from digital images. *Photogrammetric Engineering and Remote Sensing*, 56(4), 453-458.
- Entwisle, B. & Stern, P. C. (2005). *Population, land use and environment: research directions*. National Academies Press.
- ENVI. (2015). *Envi online help*. Retrieved from <http://www.exelisvis.com/language/en-s/productsservices/envi/tutorial>
- Fahmi, F., Trianda, D., Andayani, U & Siregar, B. (2018). Image processing analysis of geospatial uav orthophotos for palm oil plantation monitoring. *Journal of Physics*, 978. doi: 10.1088/1742-6596/978/1/012064
- FAO. (2002). *Origin of oil palm*. Retrieved from <http://www.fao.org/docrep/005/y4355e/y4355e03.html>
- Feng, Q., Liu, J. & Gong, J. (2015). UAV remote sensing for urban vegetation mapping using random forest and texture analysis. *Remote Sensing*, 7: 1074-1094.
- Flood, J., Bridge, P. D. & Holderness, M. (2000). *Ganoderma diseases of perennial crop*. CABI.
- Foody, G. M. & Mathur, A. (2004). Toward intelligent training of supervised image classifications: directing training data acquisition for SVM classification. *Remote Sensing of Environment*, 93, 107-117.



- Fornace, K. M., Drakeley, C. J., William, T., Espino, F. & Cox, J. (2014). Mapping infectious disease landscapes: unmanned aerial vehicles and epidemiology. *Trends in Parasitology*, 30(11), 514-519.
- Frost, V. S., Stiles, J. A., Shanmugan, K. S. & Holtzman, J. C. (1982). A model for radar images and its application to adaptive digital filtering of multiplicative noise. *IEEE Transactions on Pattern Analysis and Machine Intelligence*, 4(2), 157-166.
- Gait, F. C. (2012). Effect of pests and diseases on oil palm yield. In *Palm oil: production, processing, characterization, and uses*. Elsevier.
- Garcia-Ruiz, F., Sankaran, S., Maja, J. M., Won, S. L., Rasmussen, J. & Ehsani, R. (2013). Comparison of two aerial imaging platforms for identification of Huanglongbing-infected citrus trees. *Computers and Electronics in Agriculture*, 91, 106-115.
- Ghaiwat, S. N. & Arora, P. (2014). Detection and classification of plant leaf diseases using image processing techniques: a review. *International Journal of Recent Advances in Engineering & Technology*, 2(3), 2347-2812.
- Gopi, S., Sathikumar, R. & Madhu, N. (2014). *Advanced surveying: total station, Gis and remote sensing*. Lulu Press.
- Haniff, M. H., Zuraidah, Y. & Roslan, M. M. N. (2014). Oil palm root study at a northern region in Peninsula Malaysia. *International Journal of Agriculture Innovations and Research*, 3, 2319-1473.
- Hartley, C. W. S. (1988). *The oil palm (Elaeis guineensis Jacq.)*. England: Longman Scientific & Technical.
- Heaphy, M., Watt, M. Sw., Dash, J. P. & Pearse, G. D. (2017). UAVs for data collection - plugging the gap. *New Zealand Journal of Forestry*, 62(1), 23-30.
- Huang, X., Weng, C., Lu, Q., Feng, T. & Zhang, L. (2015). Automatic labelling and selection of training samples for high-resolution remote sensing image classification over urban areas. *Remote Sensing*, 7(12), 16023-16044.
- Hushiarian, R., Nor Azah, Y. & Sabo, W. D. (2013). Detection and control of *Ganoderma boninense*: strategies and perspectives. *Springerplus*, 2(555). doi: 10.1186/2193-1801-2-555

- Idris, A. S. (1999). *Basal stem rot (BSR) of oil palm (Elaeis guineensis Jacq.) in Malaysia: factors associated with variation in disease severity*. Ph.D thesis. Wye College, University of London, Wye, UK.
- Idris, A. S. (2004). Penyakit sawit dan kawalan. In Esnan A. G., Zin, Z. Z. & Mohd Basri, W. *Perusahaan sawit di Malaysia: satu panduan*. Selangor, Malaysia: Malaysian Palm Oil Board.
- Idris, A. S. & Rafidah, R. (2008). Enzyme linked immunosorbent assay-polyclonal antibody (ELISA-PAb). *MPOB Information Series No. 430*, pp. 4.
- Idris, A. S. (2009). Basal stem rot in Malaysia - biology, economic importance, epidemiology, detection and control. *Proceeding of the international workshop on awareness, detection and control of oil palm devastating diseases*. Kuala Lumpur Convention Centre, Malaysia.
- Idris, A. S., Mazliham, M.S., Loonis, P. & Wahid, M.B. (2010a). GanoSken for early detection of *Ganoderma*. *MPOB Information Series No. 499*, pp. 4.
- Idris, A. S., Rajiner, S., Madihah, A.Z. & Wahid, M.B. (2010b). Multiplex PCR DNA kit for early detection and identification of *Ganoderma* species in oil palm. *MPOB Information Series No. 531*, pp. 4.
- Idris, A. S., Nurrashyeda, R., Maizatul, S. M., Madihah, A. Z., Ahmad Tarmizi, M., Kushairi, D., Wan Azha, W. M. & Tony Peng, S. H. (2012). Biofertiliser Hendersonia GanoEF as biological control of *Ganoderma* in Oil Palm. *MPOB Information Series No. 595*, MPOB TT No. 508, pp. 3.
- Idris, A. S., Madihah, A. Z. & Nurrashyeda, R. (2014a). *Kawalan terkini penyakit Ganoderma sawit*. Persidangan Pekebun Kecil Peringkat Kebangsaan. Miri Sarawak.
- Idris, A. S., Mohd Shukri, I., Norman, K. A., Kushairi, A., Choo, Y. M., Mohamed, M. H., Razali, T. & Md Yid, M. S. (2014b). GanoCare™ - reducing risk of *Ganoderma* infection in oil palm. *MPOB Information Series No. 653*, MPOB TT No. 545, pp. 4.
- Izzuddin, M. A., Idris, A. S. & Nisfariza, M. N. (2013). Optimization of hyperspectral remote sensing imagery for detection of *Ganoderma* disease in oil palm. *Proceedings of the 5<sup>th</sup> MPOB-IOPRI International Seminar Posters Presentations Session V: The way forwards in pests and diseases*. Kuala Lumpur, pp. 283-288.

- Izzuddin, M. A., Idris, A. S., Nisfariza, M. N. & Ezzati, B. (2015). Spectral based analysis of airborne hyperspectral remote sensing image for detection of *Ganoderma* disease in oil palm. *Proceedings of 2015 International Conference on Biological and Environmental Science (BIOES 2015)*. Phuket, 1-3 October 2015, pp. 13-20.
- Izzuddin, M. A., Idris, A. S., Nisfariza, M. N., Nordiana, A. A., Shafri, H. Z. M. & Ezzati, B. (2017). The development of spectral indices for early detection of *Ganoderma* disease in oil palm seedlings. *International Journal of Remote Sensing*, 38(23), 6505-6527.
- Jayathunga, S., Owari, T. & Tsuyuki, S. (2018). Evaluating the performance of photogrammetric products using fixed-wing UAV imagery over a mixed conifer-broadleaf forest: comparison with airborne laser scanning. *Remote Sensing*, 10(2), 187.
- Jaybhay, J. & Shastri, R. (2015). A study of speckle noise reduction filters. *Signal & Image Processing: An International Journal*, 6(3), 71-80.
- Jensen, J. R. (2006). *Remote sensing of the environment: an Earth resource perspective*. Pearson Prentice Hall.
- Joseph, G. (2005). *Fundamentals of remote sensing*. Universities Press.
- Joshi, C., Leeuw, J. D., Skidmore, A. K. Duren, I. C. V. & Oosten, H. V. (2006). Remotely sensed estimation of forest canopy density: a comparison of the performance of four methods. *International Journal of Applied Earth Observation Geoinformation*, 8, 84-95.
- Kapilevich, B. Y., Harmer, S. W. & Bowring, H. J. (2014). *Non-imaging microwave and millimetre-wave sensors for concealed object detection*. CRC Press.
- Khairunniza-Bejo, S., Yusnida, Y., Nik Salwani, N. Y., Idris, A. S. & Izzuddin, M. A. (2015). Identification of healthy and BSR-infected oil palm trees using color indices. *International Journal of Biological, Biomolecular, Agricultural, Food and Biotechnological Engineering*, 9, 839-842.
- Kian, P. T., Kasturi, D. K. & Cracknell, A. P. (2013). Use of UK-DMC 2 and ALOS PALSAR for studying the age of oil palm trees in southern peninsular Malaysia. *International Journal of Remote Sensing*, 34(20), 7427-7446.

- Kinge, T. R. & Mih, A. M. (2011). *Ganoderma ryvardense* sp. nov. associated with basal stem rot (BSR) disease of oil palm in Cameroon. *Mycosphere*, 2(2), 179-188.
- Klemas, V. V. (2015). Coastal and environmental remote sensing from unmanned aerial vehicles: an overview. *Journal of Coastal Research*, 31(5), 1260-1267.
- Kuan, D. T., Sawchuk, A. A., Strand, T. C. & Chavell, P. (1985). Adaptive filters for images with signal-dependent noise. *IEEE Trans. Pattern Anal. Mach. Intell*, 7(2), 165-177.
- Kuan, D. T., Sawchuk, A. A., Strand, T. C. & Chavell, P. (1985). Adaptive restoration of images with speckle. *IEEE Trans. Acoust. Speech Signal Process*, 35(3), 373-383.
- Kumar, S. (2005). *Basics of remote sensing and GIS*. Firewall Media.
- Lajis, N. H., Hussein, M. Y. & Toia, R. F. (1985). Extraction and identification of the main compound present in *Elaeis Guineensis* flower volatiles. *Pertanika*, 8(1), 105-108.
- Landgrebe, D. A. (2005). *Signal theory methods in multispectral remote sensing*. John Wiley & Sons.
- Lee, J. -S. (1981). Speckle suppression and analysis for synthetic aperture radar images. *Optical Engineering*, 25(5), 255636.
- Lehmann, J. R. K., Nieberding, F., Prinz, T. & Knoth, C. (2015). Analysis of unmanned aerial system-based CIR images in forestry – a new perspective to monitor pest infestation levels. *Forests*, 6, 594-612.
- Lewis, H. G. & Brown, M. (2001). A generalized confusion matrix for assessing area estimates from remotely sensed data. *International Journal of Remote Sensing*, 22(16), 3223-3235.
- Liaghat, S., Ehsani, R., Mansor, S., Shafri, H. Z. M., Meon, S., Sankaran, S. & Azam, S. H. M. N. (2014). Early detection of basal stem rot disease (*Ganoderma*) in oil palms based on hyperspectral reflectance data using pattern recognition algorithms. *International Journal of Remote Sensing*, 35(10), 3427-3439.

- Liang, P., Shi, W. & Zhang, X. (2018). Remote sensing image classification based on stacked denoising autoencoder. *Remote Sensing*, 10(16). doi: 10.3390/rs10010016
- Lillesand, T., Kiefer, R. W. & Chipman, J. (2014). *Remote sensing and image interpretation*. John Wiley & Sons.
- Longley, P. (2005). *Geographic information systems and science (2nd ed)*. John Wiley & Sons.
- Lopes, A., Touzi, R. & Nezry, E. (1990). Adaptive speckle filters and scene heterogeneity. *IEEE Transactions on Geoscience & Remote Sensing*, 28(6), 992-1000.
- Lu, D. & Batistella, M. (2005). Exploring TM image texture and its relationships with biomass estimation in Rondônia, Brazilian Amazon. *Acta Amazonica*, 35(2), 249-257.
- Lu, D. & Weng, Q. (2007). A survey of image classification methods and techniques for improving classification performance. *International Journal of Remote Sensing*, 28(5), 823-870.
- Madiah, A. Z., Idris, A. S. & Rafidah, A. R. (2014). Polyclonal antibodies of *Ganoderma boninense* isolated from Malaysian oil palm for detection of basal stem rot disease. *African Journal of Biotechnology*, 13, 3455-3463.
- Mahdavi, S., Salehi, B., Moloney, C., Huang, W. & Brisco, B. (2017). Speckle filtering of Synthetic Aperture Radar images using filters with object-size-adapted windows. *International Journal of Digital Earth*, 11(7), 1-27.
- Mahlein, A. -K., Oerke, E. -C., Steiner, U. & Dehne, H., -W. (2012). Recent advances in sensing plant diseases for precision crop protection. *European Journal of Plant Pathology*, 133, 197-209.
- Mallinis, G., Galidaki, G. & Gitas, I. (2014). A comparative analysis of EO-1 Hyperion, Quickbird and Landsat TM Imagery for fuel type of a typical Mediterranean landscape. *Remote Sensing*, 6(2), 1684-1704.
- Mansur, M. A., Mukhtra, R. B. & Al-Doksi, J. (2014). The usefulness of unmanned airborne vehicle (UAV) imagery for automated palm oil tree counting. *Researchjournalis Journal of Forestry*, 1, 1-12.

- Maryam, K., Khairunniza-Bejo S. & Biswajeet, P. (2016). Geospatial technologies for detection and monitoring of *Ganoderma* basal stem rot infection in oil palm plantations: a review on sensors and techniques. *Geocarto International*, 6049, 1-17.
- Matese, A., Toscano, P., Di Gennaro, S. F., Genesio, Vaccari, F. P., Primicerio, J., Belli, C., Zaldei, A., Bianconi, R. & Gioli, B. (2015). Intercomparison of UAV, aircraft and satellite remote sensing platforms for precision viticulture. *Remote Sensing*, 7, 2971-2990.
- Mesas-Carrascosa, F. J., Rumbao, I. C., Berrocal, J. A. B. & Porras, A. G. F. (2014). Positional quality assessment of orthophotos obtained from sensors onboard multi-rotor UAV platforms. *Sensors*, 14(12), 22394-22407.
- Minarik, R. & Langhammer, J. (2016). Use of a multispectral UAV photogrammetry for detection and tracking of forest disturbance dynamics. *International Archives of the Photogrammetry, Remote Sensing & Spatial Information Sciences*, 41, 711-718.
- MPOB. (2015). Oil palm planted area by state as at December 2015 (hectares). Retrieved from [http://bepi.mpob.gov.my/images/area/2015/Area\\_summary.pdf](http://bepi.mpob.gov.my/images/area/2015/Area_summary.pdf)
- MPOB. (2016a). *Malaysian oil palm statistics 2015* (35<sup>th</sup> ed.). Malaysia: Ministry of Plantation Industries and Commodities, Malaysia.
- MPOB. (2016b). Monthly production of oil palm products summary 2015 (tonnes). Retrieved from <http://bepi.mpob.gov.my/index.php/statistics/production/135-production-2015/737-production-of-oil-palm-products-2015.html>
- Muhammad, R., Sahibin, A. R., Tukimat, L., Wan Mohd Razi, I. & Zulfahmi, A. R. (2015). A review of methods for detecting nutrient stress of oil palm in Malaysia. *Journal of Applied Environmental and Biological Science*, 5(6), 60-64.
- Mukherjee, I. & Sovacool, B. K. (2014). Palm oil-based biofuels and sustainability in Southeast Asia: A review of Indonesia, Malaysia, and Thailand. *Renewable and Sustainable Energy Reviews*, 37, 1-12.
- Mulla, D. J. (2013). Twenty five years of remote sensing in precision agriculture: Key advances and remaining knowledge gaps. *Biosystems Engineering*, 114, 358-371.

- Mustapha, M. R., Lim, H. S. & Mat Jafri, M. Z. (2010). Comparison of neural network and maximum likelihood approaches in image classification. *Journal of Applied Sciences*, 10, 2847-2854.
- Naher, L., Ho, C. L. & Siddiquee, S. (2012). Activities of the chitinase enzymes in the oil palm (*Elaeis guineensis* Jacq.) and their expression profiles in response to fungal infections. *Physiological and Molecular Plant Pathology*, 76(2), 96-103.
- Navulur, K. (2006). *Multispectral Image Analysis Using the Object-Oriented Paradigm*. CRC Press.
- Nisfariza, M. N., Shafri, H. Z. M., Idris, A. S., Steven, M., Boyd, D. & Mior, M. (2010). Hyperspectral sensing possibilities using Continuum Removal Index in early detection of *Ganoderma* in oil palm plantation. In: Conference on World Engineering Congress, Sarawak, Malaysia, 2010, Geomatics and Geographical Information Science, pp. 223-239.
- Nisfariza, M. N. (2012). *Early detection of Ganoderma basal stem rot disease of oil palm by hyperspectral remote sensing*. Ph.D thesis. University of Nottingham.
- Ollinger, S. V. (2011). Sources of variability in canopy reflectance and the convergent properties of plants. *New Phytologist*, 189, 375-394.
- Pan, Y., Zhang, J. & Shen, K. (2011). Crop area estimation from UAV transect and MSR image data using spatial sampling method: a simulation experiment. *Procedia Environmental Sciences*, 7, 110-115.
- Paterson, R. R. M. (2007). *Ganoderma* disease of oil palm - a white rot perspective necessary for integrated control. *Crop Protection*, 26, 1369-1376.
- Perumal, K. & Bhaskaran, R. (2010). Supervised classification performance of multispectral images. *Journal of Computing*, 2, 124-129.
- Poblete-Echeverría, C., Olmedo, G. F., Ingram, B. & Bardeen, M. (2017). Detection and segmentation of vine canopy in ultra-high spatial resolution RGB imagery obtained from unmanned aerial vehicle (UAV): a case study in a commercial vineyard. *Remote Sensing*, 9(3), 268.
- Purkis, S. J. & Klemas, V. V. (2011). *Remote sensing and global environmental change*. John Wiley & Sons.

- Purnama, S. M., Cahyawati, A. and Hutapea, D. Y. (2018). Salt pond analysis using ALOS PALSAR case study Sampang Madura-Indonesia. *IOP Conference Series: Earth Environmental Science*, 162, 012041.
- Qi, J., Inoue, Y. & Wiangwang, N. (2016). Hyperspectral remote sensing in global change studies. In Thenkabail, P. S., Lyon, J. G. & Huet, A. *Hyperspectral Remote Sensing of Vegetation*. CRC Press.
- Qiu, F., Berglund, J., Jensen, J. R., Thakkar, P. & Ren, D. (2004). Speckle noise reduction in SAR imagery using a local adaptive median filter. *GIScience and Remote Sensing*, 41(3), 244-266.
- QuestUAV. (2015). Fixed wing versus rotary wing for UAV mapping applications. Retrieved from <http://www.questuav.com/news/fixed-wing-versus-rotary-wing-for-uav-mapping-applications>
- Rango, A., Laliberte, A., Herrick, J. E., Winters, C., Havstad, K., Steele, C. & Browning, D. (2009). Unmanned aerial vehicle - based remote sensing for rangeland assessment, monitoring, and management. *Journal of Applied Remote Sensing*, 3(1). doi: 10.1117/1.3216822
- Rees, R. W., Flood, J., Hasan, Y., Potter, U. & Cooper, R. M. (2009). Basal stem rot of oil palm (*Elaeis guineensis*); mode of root infection and lower stem invasion by *Ganoderma boninense*. *Plant Pathology*, 58, 982-989.
- Richards, J. A. (2012). *Remote sensing digital image analysis: an introduction*. Springer Science & Business Media.
- Rivera-Méndez, Y. D., Rodríguez, D. T. & Romero, H. M. (2017). Carbon footprint of the production of oil palm (*Elaeis guineensis*) fresh fruit bunches in Colombia. *Journal of Cleaner Production*, 149, 743-750.
- Rizuan, C. M. Z. A., Hisham, N. H. & Samsudin, A. (2013). Role of pollinating weevil (*Elaeidobius kamerunicus*), seasonal effect and its relation to fruit set in oil palm area of FELDA. Paper presented at PIPOC 2013 Conference, November 19-21, KLCC, Kuala Lumpur, Malaysia,
- Roslan, M. M. N. & Hanif, M. H. (2004). Botani sawit. In Esnan, A. B., Zin Zawawi, Z. & Basri, M. W. *Perusahaan sawit di Malaysia: satu panduan*. Selangor, Malaysia: Malaysian Palm Oil Board.



- Roslan, A. & Idris, A. S. (2012). Economic impact of *Ganoderma* incidence on Malaysian oil palm plantation: a case study in Johor. *Oil Palm Industry Economic Journal*, 12(1), 24-30.
- Saberioon, M. M., Amin, M. S. M., Anuar, A. R., Gholizadeh, A., Wayayok, A. & Khairunniza-Bejo, S. (2014). Assessment of rice leaf chlorophyll content using visible bands at different growth stages at both the leaf and canopy scale. *International Journal of Applied Earth Observation and Geoinformation*, 32, 35-45.
- SALCRA (Sarawak Land Consolidation and Rehabilitation Authority). (2012). *Pests and Diseases Control*. Retrieved from <http://www.salcra.gov.my/en/sustainable-plantation/pest-diseases-control.html>
- Sanderson, F. R. (2005). An insight into spore dispersal of *Ganoderma boninense* on oil palm. *Mycopathologia*, 159, 139-141.
- Santoso, H., Gunawan, T., Jatmiko, R. H., Darmosarkoro, W. & Minasny, B. (2011). Mapping and identifying basal stem rot disease in oil palms in North Sumatra with QuickBird imagery. *Precision Agriculture*, 12(2), 233-248.
- Sarode, M. V. & Deshmukh, P. R. (2011). Reduction of speckle noise and image enhancement of images using filtering technique. *International Journal of Advancements in Technology*, 2(1), 30-38.
- Schellberg, J., Hill, M. J., Gerhards, R., Rothmund, M. & Braun, M. (2008). Precision agriculture on grassland: Applications, perspectives and constraints. *European Journal of Agronomy*, 29, 59-71.
- Shafri, H. Z. M. & Izzuddin, M. A. (2008). *Hyperspectral signal analysis for detecting disease infection in oil palms*. Computer and Electrical Engineering. International Conference, Phuket, Thailand.
- Shafri, H. Z. M., Izzuddin, M. A., Idris, A. S. & Nisfariza, M. N. (2011). Spectral discrimination of healthy and *Ganoderma*-infected oil palms from hyperspectral data. *International Journal of Remote Sensing*, 32, 7111-7129.
- Shafri, H. Z. M., Hamdan, N. & Izzuddin, M. A. (2012). Detection of stressed oil palms from an airborne sensor using optimized spectral indices. *International Journal of Remote Sensing*, 33(14), 4293-4311.

- Shi, Z. & Fung, K. B. (1994). A comparison of digital speckle filters. In *Geoscience and Remote Sensing Symposium, 1994. IGARSS '94. Surface and Atmospheric Remote Sensing: Technologies, Data Analysis and Interpretation, Pasadena, USA*. doi: 10.1109/IGARSS.1994.399671
- Shome, P. & Sharma, P. (2015). *Emerging economies: food and energy security, and technology and innovation*. Springer.
- Singh, G. (1991). *Ganoderma* – the scourge of oil palm in the coastal areas. *The Planter*, 67, 421-444.
- Smith, R. B. (2012). *Introduction to Remote Sensing of Environment*. MicroImages Inc.
- Story, M. & Congalton, R. G. (1986). Accuracy assessment: a user's perspective. *Photogrammetric Engineering and Remote Sensing*, 52, 397-399.
- Susanto, A., Sudharto, P. S. & Purba, R. Y. (2005). Enhancing biological control of basal stem rot disease (*Ganoderma boninense*) in oil palm plantations. *Mycopathologia*, 159, 153-157.
- Takeuchi, W. & Khiabani, P. H. (2017). Supporting efficient management of oil palm plantation using remote sensing (RS), unmanned aerial vehicle (UAV), geographic information system (GIS) and global navigation satellite system (GNSS). International Conference on Big Data Applications in Agriculture (ICBAA2017). 5-6 December 2017.
- Tan, K. C., Lim, H. S. & Mat Jafri, M. Z. (2011). Comparison of neural network and maximum likelihood classifiers for land cover classification using Landsat multispectral data. IEEE Conference on Open Systems (ICOS2011), 25-28 September 2011. Langkawi, Malaysia.
- Tona, E. (2017). *Contributions on advanced automation for selective protection treatments on specialty crops*. PhD Thesis. Milan: Universitas Studiorum Mediolanensis.
- Turner, P. D. (1981). *Oil palm diseases and disorders*. London: Oxford University Press.
- Turner, P. D. & Gillbanks, R. A. (2003). *Oil palm cultivation and management*. Kuala Lumpur, Malaysia: Incorporated Society of Planters.

- Venkateswarlu, B., Shanker, A. K., Shanker, C. & Maheswari, M. (2011). *Crop stress and its management: perspectives and strategies*. Springer Science & Business Media.
- Verheye, W. (2010). Growth and production of oil palm. In: Verheye, W. (ed.), *Land use, land cover and soil sciences. Encyclopedia of Life Support Systems (EOLSS), UNESCO-EOLSS Publishers, Oxford, UK*. Retrieved from: <http://www.eolss.net>
- Viera, A. J. & Garrett, J. M. (2005). Understanding interobserver agreement: the Kappa statistic. *Family Medicine*, 37(5), 360-363.
- Vollmann, J. & Rajcan, I. (2009). *Handbook of plant breeding*. New York: Springer.
- Wang, G. & Weng, Q. (2013). *Remote sensing of natural resources*. CRC Press.
- West, J. S., Bravo, C., Oberti, R., Lemaire, D., Moshou, D. & McCartney, H. A. (2003). The potential of optical canopy measurement for targeted control of field crop diseases. *Annual Review Phytopathol*, 41, 593-614.
- Wong, L. C., Bong, C. F. J. & Idris, A. S. (2012). *Ganoderma* species associated with basal stem rot disease of oil palm. *American Journal of Applied Sciences*, 9, 879-885.
- Yuan, L., Zhang, J., Shi, Y., Nie, C., Wei, L. & Wang, J. (2014). Damage mapping of powdery milder in winter wheat with high-resolution satellite image. *Remote Sensing*, 6(5), 3611-3623.
- Yuan, H., Yang, G., Li, C., Wang, Y., Liu, J., Yu, H., Feng, H., Xu, B., Zhao, X. & Yang, X. (2017). *Remote Sensing*, 9, 309.
- Yue, J., Lei, T., Li, C. & Zhu, J. (2012). The application of unmanned aerial vehicle remote sensing in quickly monitoring crop pests. *Intelligent Automation and Soft Computing*, 18(8), 1043-1052.
- Zarco-Tejada, P. J., Mateos, L, Fereres, E. & Villalobos, F. J. (2016). New tools and methods in agronomy. In Villalobos, F. & Fereres, E. *Principles of Agronomy for Sustainable Agriculture*. Springer, Cham.

Zhang, M., Qin, Z. & Liu, X. (2005). Remote sensed spectral imagery to detect late blight in field tomatoes. *Precision Agriculture*, 6(6): 489-508.

Zhang, Z. X. (2014). *Native Vegetation Classification Using Remote Sensing Techniques: A Case Study of Dairy Flat Regrowth Bush by Using the AUT Unmanned Aerial Vehicle*. MSc Thesis. Auckland University of Technology, New Zealand.

University of Malaya

## LIST OF PUBLICATION AND PAPER PRESENTED

Ezzati B., Nisfariza, M. N., Izzuddin, M. A., Idris, A. S. and Siti Aisyah, A. (2016). Supervised classification techniques for mapping the *Ganoderma* disease using unmanned aerial vehicle. *4th Kuala Lumpur International Agriculture, Forestry and Plantation (KLIAFP) Proceeding*. Hotel Putra, Kuala Lumpur, Malaysia. 12-13 December 2016, pp. 220-230.

Izzuddin, M. A., Idris, A. S., Nisfariza, M. N., Nordiana, A. A., Shafri, H. Z. M. and Ezzati, B. (2017). The development of spectral indices for early detection of *Ganoderma* disease in oil palm seedlings. *International Journal of Remote Sensing*, 38(23), 6505-6527.

University of Malaysia